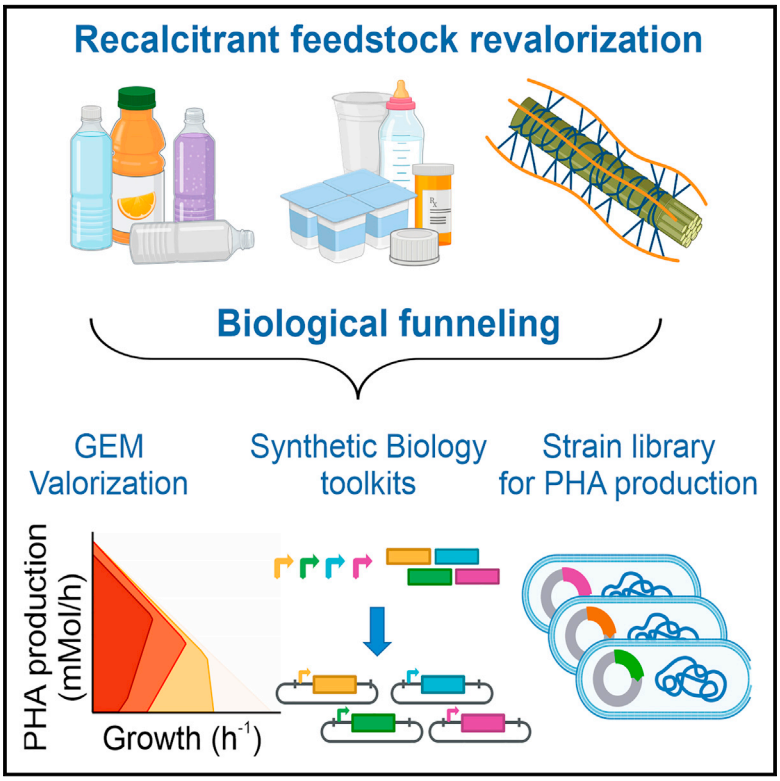
Cell Reports

Article

A model-driven approach to upcycling recalcitrant feedstocks in *Pseudomonas putida* by decoupling PHA production from nutrient limitation

Graphical abstract



Highlights

- Model-driven carbon flux rerouting enhances PHA production from complex compounds
- Removal of regulatory constraints overcomes nutrient limitation for PHA production
- Up to 46% of PHA/CDW was achieved under a balanced C/N ratio

Authors

Maria-Tsampika Manoli, Álvaro Gargantilla-Becerra, Carlos del Cerro Sánchez, Virginia Rivero-Buceta, M. Auxiliadora Prieto, Juan Nogales

Correspondence

auxi@cib.csic.es (M.A.P.), jnogales@cnb.csic.es (J.N.)

In brief

Manoli et al. present a library of model-driven optimized *P. putida* strains able to upcycle recalcitrant polymers toward high-value-added products, polyhydroxyalkanoates. Through strategic metabolic flux rerouting and removal of intrinsic regulatory constraints, high PHA yields were successfully achieved by effectively decoupling production from nutrient limitations.

Manoli et al., 2024, Cell Reports *43*, 113979
April 23, 2024 © 2024 The Authors.
https://doi.org/10.1016/j.celrep.2024.113979

CellPress

Cell Reports

CellPress
OPEN ACCESS

Article

A model-driven approach to upcycling recalcitrant feedstocks in *Pseudomonas putida* by decoupling PHA production from nutrient limitation

Maria-Tsampika Manoli,[1,2] Álvaro Gargantilla-Becerra,[2,3] Carlos del Cerro Sánchez,[1,2] Virginia Rivero-Buceta,[1,2] M. Auxiliadora Prieto,[1,2,*] and Juan Nogales[2,3,4,5,*]

[1]Polymer Biotechnology Group, Department of Microbial and Plant Biotechnology, Margarita Salas Center for Biological Research (CIB-CSIC), 28040 Madrid, Spain

[2]Interdisciplinary Platform for Sustainable Plastics towards a Circular Economy-Spanish National Research Council (SusPlast-CSIC), Madrid, Spain

[3]3Systems Biotechnology Group, Department of Systems Biology, Centro Nacional de Biotecnología, CSIC, Madrid 28049, Spain

[4]CNB DNA Biofoundry (CNBio), CSIC, Madrid, Spain

[5]Lead contact

*Correspondence: auxi@cib.csic.es (M.A.P.), jnogales@cnb.csic.es (J.N.)

https://doi.org/10.1016/j.celrep.2024.113979

SUMMARY

Bacterial polyhydroxyalkanoates (PHAs) have emerged as promising eco-friendly alternatives to petroleum-based plastics since they are synthesized from renewable resources and offer exceptional properties. However, their production is limited to the stationary growth phase under nutrient-limited conditions, requiring customized strategies and costly two-phase bioprocesses. In this study, we tackle these challenges by employing a model-driven approach to reroute carbon flux and remove regulatory constraints using synthetic biology. We construct a collection of *Pseudomonas putida*-overproducing strains at the expense of plastics and lignin-related compounds using growth-coupling approaches. PHA production was successfully achieved during growth phase, resulting in the production of up to 46% PHA/cell dry weight while maintaining a balanced carbon-to-nitrogen ratio. Our strains are additionally validated under an upcycling scenario using enzymatically hydrolyzed polyethylene terephthalate as a feedstock. These findings have the potential to revolutionize PHA production and address the global plastic crisis by overcoming the complexities of traditional PHA production bioprocesses.

INTRODUCTION

Microorganisms are key players in industrial biotechnology, and they have been widely used for the production of valuable bioproducts such as fine chemicals, polymers, and biofuels, among others. However, to render a wild-type strain into an industrially efficient microbial platform is costly and, in most cases, uncertain.[1] The design-build-test-learn (DBTL) cycle principles arose in pursuit of this, facilitated by the increasingly improving capabilities in the synthetic biology field and an exponentially adopted metabolic engineering framework. DBTL represents a more efficient and systematic approach to strain construction (Figure 1).[2,3] In fact, over the last years, several efforts have been focused on optimizing strain performance as far as it concerns titer, rate, and yield of production.[4]

To achieve these ambitious objectives, a holistic approach is needed for the final design of the microbial chassis. This is because metabolic engineering and synthetic biology efforts often face limitations due to the introduction of non-native biochemical transformations into the host metabolic networks. To address these challenges, genome-scale metabolic models (GEMs) and constraint-based reconstruction and analysis (COBRA) methods are commonly employed to predict the optimal distribution of metabolic fluxes.[5] These *in silico* tools rely on a detailed understanding of the microorganism's metabolic network and the maintenance of a mass balance during steady-state growth. GEMs and COBRA methods have proven to be valuable in multiple applications, including the accurate prediction of byproduct secretions in organisms such as *Escherichia coli* and *Saccharomyces cerevisiae*.[6,7]

Over the past decade, one crucial design principle for metabolic engineering and computational strain construction is to couple cellular growth with the production of a desired functionality (metabolite/growth).[8] This approach ensures that the synthesis of the target product occurs concurrently with cell growth, optimizing overall productivity. This coupling can be achieved by integrating the production pathway with essential cellular processes that are required for growth. Therefore, growth of the organism becomes a driving force of production.[9] Overall, growth-coupled overproducer microbial strains provide multiple advantages such as increased productivity, enhanced substrate utilization, reduced byproduct formation, increased strain stability, and

This is an open access article under the CC BY-NC license (http://creativecommons.org/licenses/by-nc/4.0/).

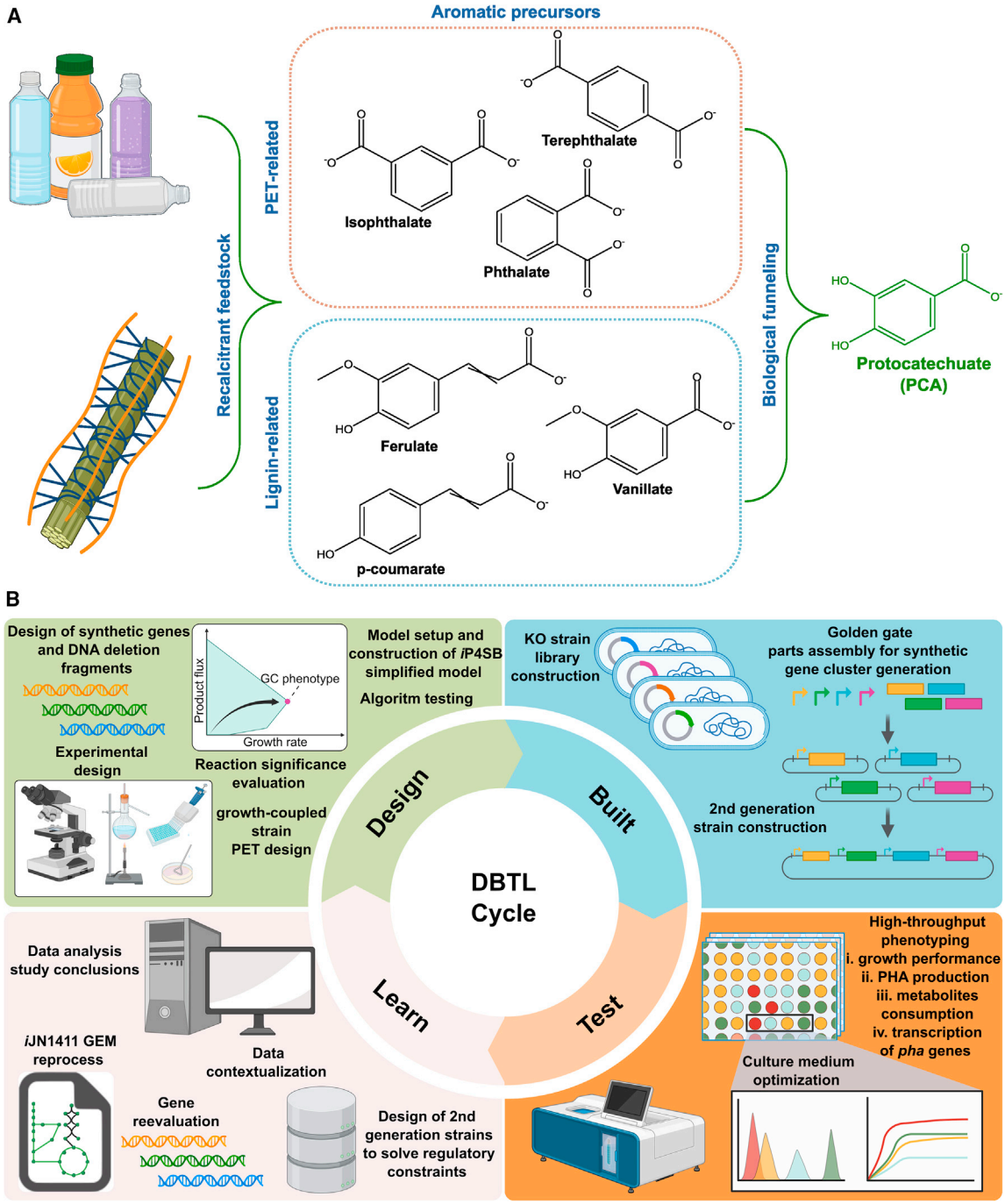


Figure 1. Workflow used in this study

(A) Schematic representation of the funneling concept utilized in this study to connect a diverse range of lignin- and plastic-derived compounds to protocatechuate (PCA). The strategy involves utilizing PCA as a crucial intermediate that bridges the gap between recalcitrant compounds and the central metabolism through the β-ketoadipate pathway.

(B) DBTL cycle design principles used in this work. The BioRender platform was used for figure designing.

flexibility in strain optimization. In the context of GEMs, a large number of algorithms have been developed to predict and engineer growth-coupled chemical production.[5,10] A variety of *E. coli* mutant strains have successfully been constructed by using growth-coupling approaches for the production of lactic acid,[11] ethanol,[12] malonyl-CoA,[13] and itaconic acid,[14] among others.

In the context of the current climate crisis and the emerging circular economy, a major goal is the replacement of current

crude-oil-based plastics with more sustainable and biodegradable alternatives. Polyhydroxyalkanoates (PHAs) are native products of many bacteria and can be considered as an alternative to fossil-based plastics, with wide applications in medical and material fields.[15,16] PHAs are stored as intracellular reserve storage granules, and they can play a role as sinks for carbon and reducing equivalents.[17,18] The hydrophobic granules are coated by granule-associated proteins (i.e., synthases, depolymerase, phasins, and others) that are involved in PHA production and its complex regulation.[19,20] PHA production presents, however, a significant challenge due to their association with the stationary growth phase and the requirement for nutrient limitation, typically nitrogen, phosphorus, or oxygen, combined with carbon excess.[16] This key constraint is an important bottleneck in the production of PHA, as it requires a two-step bioprocess. During the first phase, the bacteria are provided with an abundant supply of nutrients, particularly carbon, to allow them to multiply and accumulate biomass. This phase ensures that a substantial population of bacteria is available for the subsequent production phase. Once the desired cell density is achieved, the second production phase begins by limiting the availability of certain nutrients, particularly nitrogen, while still maintaining sufficient levels of other nutrients necessary for PHA synthesis. While the two-step bioprocess effectively produces PHA, it comes with important challenges including the need for separate growth and production phases, which results in energy-intensive and resource-consuming processes.[20,21]

Several bacteria genera have attracted much interest as efficient biocatalysts for PHA production including halophiles due to their ability to use cheap raw materials as feedstock, thus decreasing fermentation costs.[22] However, the absence of high-quality GEMs for model halophilic bacteria and other promising PHA producers hinders the utilization of these microorganisms in computational-driven growth-coupled strategies. In contrast, pseudomonad species are an interesting chassis for implementing such strategies. Beyond interest due to their metabolic versatility, adaptability to endogenous and exogenous stresses, fast growth, genetic accessibility, and high productivities,[23,24] model strains such as *Pseudomonas putida* KT2440 have become promising organisms for biotechnological, environmental, and industrial applications.[25] Furthermore, KT2440 is also a medium-chain-length producer and has a high-quality GEM available.[26]

The PHA metabolism in *Pseudomonas* spp. is mediated through the PHA synthases (PhaC) and the PHA depolymerase (PhaZ) that synthesize and degrade the PHA, respectively.[17,20] PhaZ continuously releases the 3-hydroxyfatty acids that are either catabolized via fatty acid metabolism or reincorporated into PHA granules by the action of the synthases. The PHA metabolic machinery is closely connected to the β-oxidation pathway and *de novo* fatty acid biosynthesis for providing the precursors of PHA synthases. Therefore, β-oxidation pathway performs the conversion of fatty acids (i.e., PHA structure-related carbon sources), and *de novo* fatty acid biosynthesis uses non-fatty acids (i.e., glucose, glycerol) substrates to (R)-HA-CoAs precursors for mcl-PHA production.[27] PHA metabolism is additionally controlled via a complex multilevel regulatory network driven by global regulators linked to central carbon metabolism and *pha*-specific regulators in the *pha* cluster.[16]

Despite the huge effort put forth so far for the production of PHA using related[20,28,29] and easily fermentable carbon sources,[30,31] the new circular economy paradigm aims toward the production of these bioplastics from recalcitrant material such as lignin and petrol-based plastics like polyethylene terephthalate (PET) and polyurethane.[32,33] To overcome these limitations, the biological funneling concept based on the ability of some bacterial species to converge a plethora of these heterogeneously derived aromatics into a few central intermediates like catechol and protocatechuate (PCA) could be an interesting strategy.[34,35] These intermediates are finally cleaved and metabolized via the β-ketoadipate pathway to access the central carbon catabolism (Figure 1).[36,37]

In this study, we addressed the challenge of developing a more efficient method for single-step PHA production using recalcitrant carbon sources as feedstock, including PET hydrolysates. For this, we employed a model-guided growth-coupled strategy assisted by synthetic biology. By employing this innovative approach, we successfully circumvented nutrient limitations and effectively redirected the central metabolism to optimize the carbon flux toward PHA biosynthesis during the growth phase. Our findings highlight the potential of this strategy to revolutionize PHA production processes, offering a sustainable and streamlined solution to address the global plastic crisis.

RESULTS

Model setup and construction of a PET-reduced metabolic model

P. putida KT2440 is not able to grow naturally either on PET or on its aromatic monomeric constituents derived from its hydrolysis, e.g., terephthalic acid (TPA) and ethylene glycol (EG) as the sole carbon source. Therefore, we used an updated *P. putida* model based on *i*JN1411[26,38] accounting for the metabolism of PET and other plastics while harboring a reduced biomass objective function. The resulting model, *i*JNP4SB,[26,33] has been successfully used previously to assess the potential of this strain for plastic upcycling. PET metabolism was simulated using a PET uptake rate of 3.78 mmol gDW^{-1} h^{-1} that was equivalent to glucose uptake in terms of carbon content.

In order to reduce the computational complexity of the analysis, we proceeded to simplify the *i*JNP4SB model and obtain a reduced knockout (KO) reaction list following the workflow shown in Figure 2. Briefly, the reduced model was constructed by applying two consecutive steps, e.g., model simplification and model reduction (see "Model-driven design of growth-coupled PHA strains" in the STAR Methods). These approaches allowed us to significantly decrease the number of reactions suitable to be deleted. The reduced/simplified PET model contained 1,385 reactions and 1,033 metabolites, while the KO reaction list was reduced to 233 reactions (https://doi.org/10.6084/m9.figshare.23760606.v1). Next, this reduced PET model was the basis for the identification of growth-coupled PHA designs using PET as the carbon source.

Model-driven design of PHA-overproducing strains using PET as carbon source

The identification of *in silico* growth-coupled overproducing PHA designs using PET as the sole carbon source was addressed by

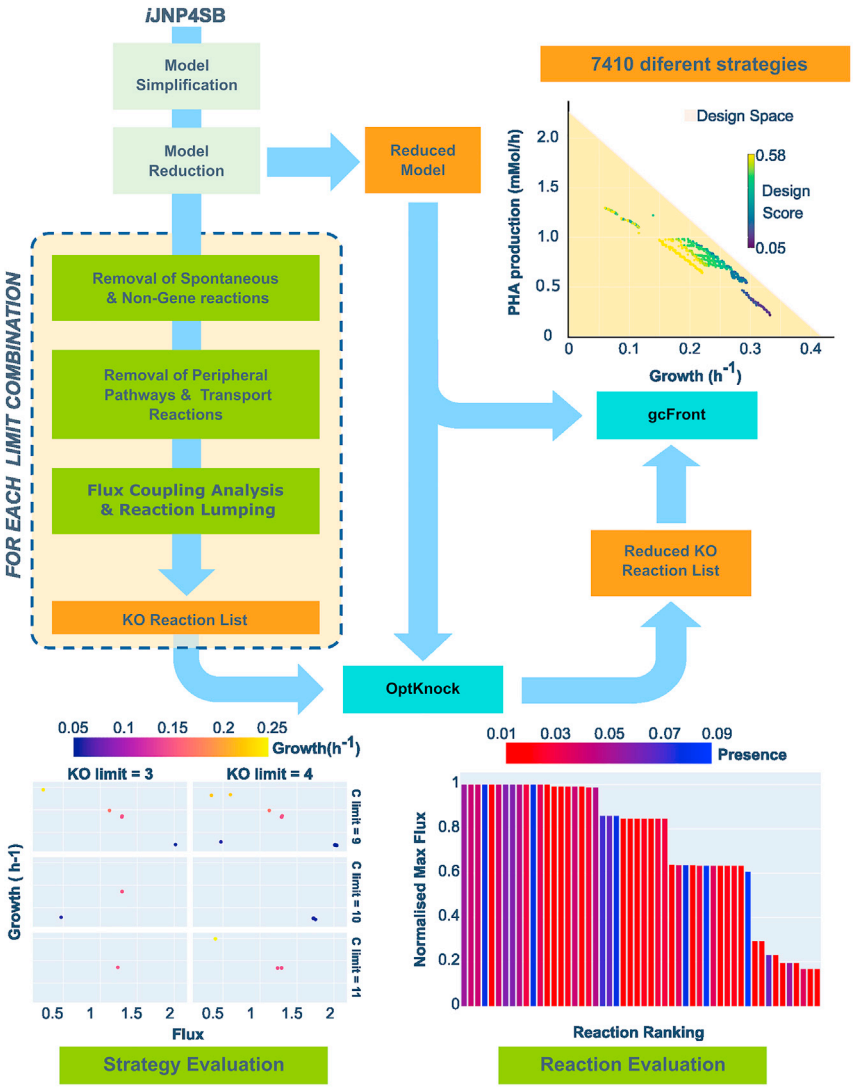


Figure 2. Schematic representation of the strain-design computational workflow developed in this work

The updated *i*JNP4SB model was first simplified and reduced as described in the STAR Methods, resulting in the generation of a reduced model. The generation of the reduced KO reaction list involved the execution of OptKnock with varying KO and carbon (C) limits. Iteratively following the steps outlined within the yellow box, each parameter combination resulted in a distinct candidate list.

applying the gcFront algorithm following the established parameters described in Table S2 (see "Model-driven design of growth-coupled PHA strains" in the STAR Methods). The gcFront algorithm is designed to explore KO strategies that simultaneously maximize cell growth, product synthesis, and coupling strength through tri-level optimization. Utilizing a genetic algorithm, gcFront can efficiently generate numerous alternative optimal and suboptimal designs on the Pareto surface in a single run.[39] We successfully generated a total of 7,410 distinct strain designs, thus comprehensively exploring the metabolic landscape for PHA production from PET (Figures 2 and 3A). We next conducted a thorough analysis to identify the most promising designs based on three key criteria: (1) PHA yield, (2) biomass-coupled product yield (BCPY), and (3) coupling strengths. From the pool of designs with the highest design scores, we specifically focused on PET4. This particular design exhibited outstanding performance, attaining the highest BCPY score (0.17 mmol PHA gDW^{-1}) while enabling a growth rate above 0.10 h^{-1} and a PHA yield above 1.00 mmol gDW^{-1} h^{-1} and displaying significant coupling strength (Figure 3A).

To gain deeper insights into the metabolic potential and practical applicability of PET4, we assessed its performance growing on PET through dynamic flux balance analysis (Figure 3B). This computational simulation provided valuable predictions, including its theoretical growth curve, growth rate, PHA production, and BCPY (Figures 3B; Table S3). Notably, the model-based predictions indicated that the engineered *P. putida* strain based on the PET4 design could potentially accumulate over 50% of its biomass as PHA, even without a nitrogen limitation (Table S3). Taking into account the feasibility of PET degradation and the advanced research on PET hydrolases, the PET4 growth-coupled design represented an encouraging starting point for further *in vivo* implementation.[32,40–42]

Metabolic contextualization of PET4 design

The PET4 design involved the deletion of 16 reactions, which required the removal of 27 genes (Table S3). This extensive number of genetic modifications posed a significant challenge for its *in vivo* implementation. In order to identify the minimal number of KOs still resulting in an efficient growth-coupled design, we computationally evaluated the impact of each deletion in terms of PHA production, coupling strength, and biomass production (Figure 3C; Table S4). By this effort, we classified the KOs into three major groups: (1) minimal deletions, those essential for coupling PHA to growth (ORNCD, ICL, ICDHyr, and MALS), (2) complementary deletions, which contribute significantly either to coupling strength or to PHA production (FORGLULH2, MCITL2, PPCSCT, and SUCOAS), and (3) dispensable deletions, those providing only negligible improvement on coupling strength and/or PHA production (UPPN, ALATA_L, ALAR. RBK, OARGDC, ABUTD, PDHcr, and PDHbr) (Figure 3C; Table S4).

Based on this analysis, it was feasible to identify three possible growth-coupled designs accounting for an increasing

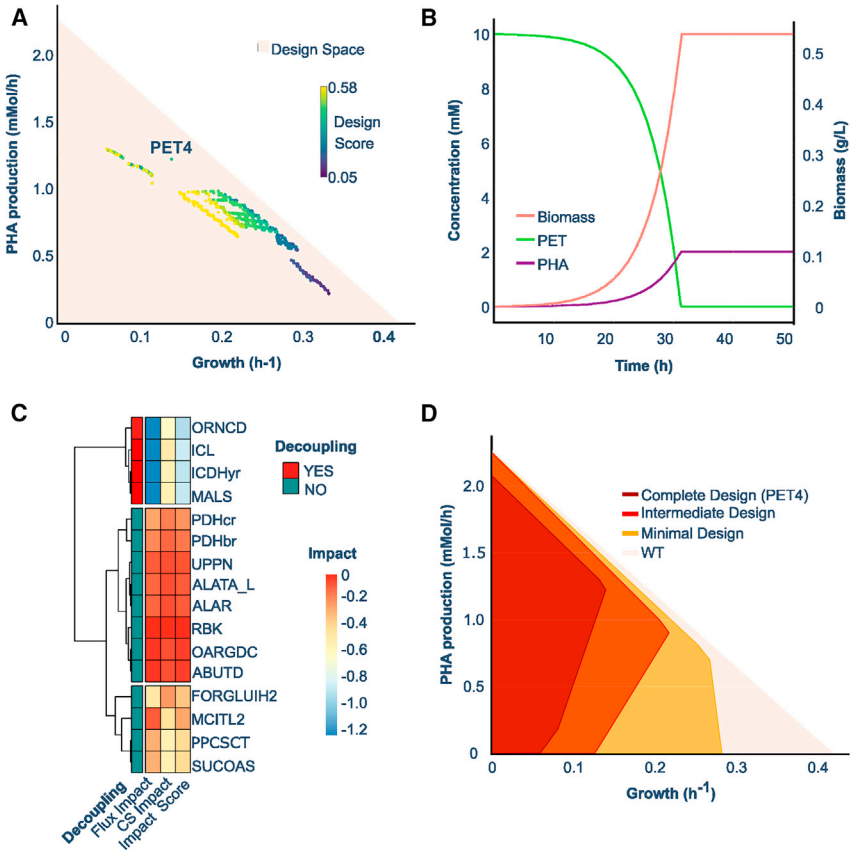


Figure 3. *In silico* manual curation for identifying the best growth-coupled candidates

(A) Production envelopes of several *in silico* designs depicted within the wild-type (WT) strain. The designs are color coded based on our proposed design score, which considers equally coupling strength (as defined in the gcFront) and biomass-coupled product yield (BCPY).

(B) Assessment of PET4 performance using dynamic flux balance analysis (FBA), biomass (red), PET consumption (green), and PHA production (purple).

(C) Clustered impact ranking of individual reactions for PET4 performance evaluation.

(D) Production envelopes of WT strain and three different designs derived from PET4/complete are shown. For more details concerning the nomenclature, please refer to Table S4.

number of KOs: minimal, intermediate, and complete (Figure 3D; Table S3). The production envelope profiles of such designs harbor 4, 8, and 16 KO reactions, respectively (Figure 3D). Despite the significantly lower number of KOs (8) of the intermediate design, it retained the capability to produce a significant amount of PHA. Remarkably, the intermediate design achieved nearly 95% of the biomass-coupled product (BPCY) observed in the complete design (Figure 3D). A comparison of the properties of the three proposed growth-coupled designs is provided in Table S3.

The detailed carbon flux *in silico* analysis of the intermediate PET4 design showed that, as expected, the TPA derived from PET was further catabolized via PCA through the β-ketoadipate pathway, yielding succinyl-CoA and acetyl-CoA (Figure S1). EG was predicted to be catabolized via glycolate to yield L-serine. Then, it was completely oxidized to CO_2 via the oxidative glycine cycle (Figure S1). Interestingly, this non-conventional oxidation cycle replaced the oxidative branch of TCA as a source of reducing power. Overall, the model predicted that succinate and EG were mainly used as biomass building blocks and energy sources, while the *de novo* fatty acid biosynthesis pathway acted as the main acetyl-CoA sink driving PHA production coupled to growth (Figure S1). Given these promising properties, the intermediate design emerges as a favorable candidate for *in vivo* implementation (Table S3).

Construction of a PHA-overproducing *P. putida* strain based on PET4 design

In order to construct the PET4 design, we sequentially deleted the gene(s) encoding the reactions identified. We relied on a system for individual gene deletions (pK18*mobsacB*) and performed successive rounds of gene deletions. A logical order to delete the genes was planned based on the predicted impact of each deletion on PHA production and/or growth performance (Table S4). To facilitate the understanding, a workflow of the mutants' construction and the information concerning the deleted reactions/genes is shown in Figure 4.

The first three deleted reactions were those responsible for blocking the succinate metabolism: 2-methylisocitrate lyase, propionyl-CoA:succinate-CoA transferase, and succinyl-CoA synthetase. The next knocked out reactions were isocitrate lyase and malate synthase, responsible for the *glyoxylate* cycle, thus avoiding the consumption of acetyl-CoA via this anaplerotic pathway. The subsequent deletion was isocitrate dehydrogenase, which, when taken together with the previous five deletions, was expected to eliminate a substantial portion of the carbon flux through the TCA cycle. It is worth mentioning here that *P. putida* KT2440 has two isocitrate dehydrogenases, namely the dimeric ICD (PP_4011) and the monomeric IDH (PP_4012). Despite multiple attempts, the deletion of the monomeric PP_4012 proved unfeasible. Interestingly, IDH could not be deleted even in the wild-type strain despite the presence of ICD, thus suggesting an unknown role of IDH in *P. putida* other than its participation in TCA. This inability to delete IDH may sustain some carbon flux through the TCA cycle, potentially diminishing the coupling strength of our final strain, as illustrated below.

The seventh reaction to be sequentially deleted was the PHA depolymerase, PhaZ, which, although it was not part of the intermediate PET4 designs, was expected to allow stable PHA accumulation, as we have previously shown.[20] The

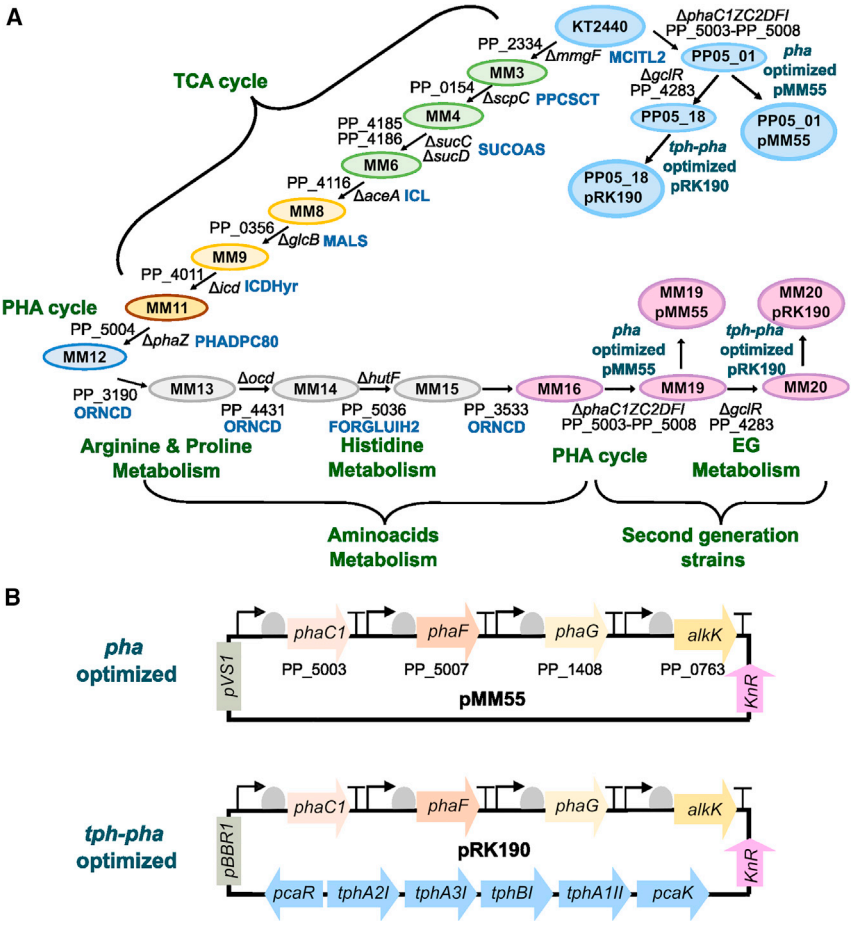


Figure 4. KO mutant strains and plasmid used in this study

(A) Workflow of mutant strategy construction. The outlined strategy involved constructing KO mutants in the background of *P. putida* KT2440. These mutants, denoted as MMx, targeted various metabolic pathways, including succinate, glyoxylate shunt, isocitrate dehydrogenase, PHA cycle, amino acids, and EG metabolism. The blue letters represent model reactions (refer to Table S4 for nomenclature details). Mutants in WT and growth-coupled backgrounds are differentiated by blue and pink colors, respectively.

(B) Simplified plasmid structure for *pha*- and *tph-pha*-optimized production.

last deletions affected ornithine cyclodeaminase (PP_3190, PP_3533, PP_4431; *ocd* genes) and formiminoglutamate deiminase (PP_5036; *hutF* gene). These last iterations were required to avoid alternative metabolism of acetyl-CoA and acetate secretion via amino acid (i.e., arginine and proline) metabolism. The final strain, MM16, was subsequently used for PHA production. Overall, in the MM16 background, we successfully managed to sequentially delete seven out of the eight key reactions from the PET4 intermediate design, and it is also likely that the flux through the remaining reaction (i.e., isocitrate dehydrogenase) was reduced.

PET4 designs overproduce PHA in the absence of nutrient limitations

After implementation, the ideal scenario was to phenotypically evaluate the growth and PHA production capacity of the constructed strains under similar conditions to those previously simulated (PET). However, *P. putida* KT2440 cannot metabolize PET or its hydrolyzed monomers, such as TPA. Following the biological funneling concept (Figure 1), we selected PCA, a key intermediate in the degradation of PET via TPA, as an optimal surrogate carbon source. However, since PCA is highly unstable and rapidly oxidizes under working conditions, we utilized 4-hydroxybenzoate (4HBz) as a proxy since it is metabolized via PCA. Finally, to facilitate the screening process and the production of PHA from PHA-unrelated carbon sources, we added octanoate as a direct source of acetyl-CoA for putative growth-coupled cells.[30]

Under this nutritional scenario, we proceeded with the phenotypic analysis of the KO strains (Figure 5; Table S5). Notably, we identified the deletion of succinyl-CoA synthase, *sucC-sucD* (*sucC,D*), and isocitrate lyase, *aceA*, as the key KO reactions that resulted in a significant increase in PHA content (Figure 5A). The deletion of *sucC,D* was especially important, as it led to a substantial increase in PHA production from 5% PHA/cell dry weight (CDW) in the MM4 strain to 22% PHA/CDW in the MM6 strain (Figure 5A; Table S5). The deletion of isocitrate lyase has previously been reported to improve PHA production[43]; however, the lack of *sucC,D* genes has not, so far, been related to improved PHA production. The remaining KOs resulted in only slight improvements in PHA production compared to the MM8 strain (32% PHA/CDW). It is reasonable to speculate that these KOs may contribute to increased coupling strength as predicted *in silico*.

Overall, we showed that the model-guided MM16 strain was able to efficiently produce PHA, reaching up to 33.7% of PHA/CDW production, under a balanced growth condition (M63 minimal medium supplemented with 3 mM octanoate 5 mM 4HBz) without the implementation of nitrogen limitation.

β-Oxidation pathway is the predominant PHA pathway in MM16 strain

PHA can be produced either via β-oxidation or *de novo* fatty acid synthesis (see the introduction section for more details as well as Figure 5C). Since 4HBz is a non-PHA-related carbon source, it would be expected that the *de novo* fatty acid pathway serves as the primary source of PHA precursors. However, in the nutritional scenario analyzed, there is a mixture of carbon sources (4HBz and octanoate); thus, it becomes challenging to determine the specific pathway utilized for PHA production in the MM16 strain.

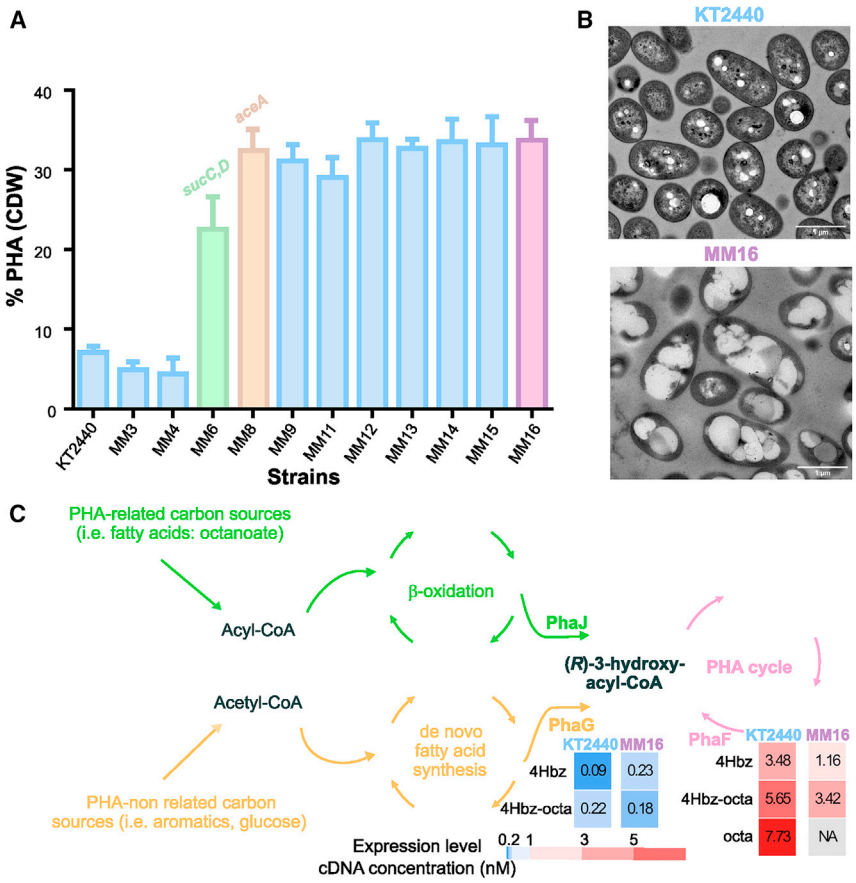


Figure 5. Growth-coupled mutants' construction and corresponding physiological analyses

(A) The PHA (%CDW) content after 24 h of growth in M63 minimal medium supplemented with 3 mM octanoate (octa) and 5 mM 4-hydroxybenzoate (4HBz; C/N ratio: 2 mol/mol) in the different deletion mutant backgrounds is shown. The data correspond to the mean values and standard deviations of three independent biological replicates with two technical replicates for the methanolysis process.

(B) Electronic microscopy pictures of KT2440 and MM16 strains after 24 h of growth under the abovementioned conditions. The scale bar of the pictures represents 1 μm.

(C) Schematic representation of the real-time qPCR experiments under M63 5 mM 4HBz, M63 5 mM 4HBz + 3 mM octa (4HBz-octa), and M63 15 mM octa (control). Heatmap representation of the expression levels in nM cDNA concentration of key pha genes (i.e., phaG and phaF) in KT2440 and MM16 strains. For more details concerning the nomenclature, please refer to Figure 4 and Table S4.

To assert the metabolic pathway supplying the precursors for PHA production observed in MM16, we took advantage of the fact that when a fatty acid is used as the carbon source in every round of β-oxidation, an acetyl-CoA molecule is lost. This would allow us to easily identify the monomeric composition of the resulting polymer.[28] Subsequently, we replaced octanoate with the odd fatty acid 10-undecenoate and monitored the PHA monomer patterns produced. If odd-chain monomers were obtained, then this would unequivocally indicate that they came from the β-oxidation; however, if even-chain monomers appeared, then this would suggest that they came from the *de novo* fatty acid synthesis.

Following this premise, the PHA content was quantified in KT2440 and MM16 strains after 24 h of growth using 3 mM 10-undecenoic acid and 5 mM 4HBz as carbon sources (Table S6). However, no significant differences were observed as far as the PHA monomeric pattern between the strains is concerned. Therefore, since only odd monomers were observed, it could be concluded that the pathway used for PHA synthesis in MM16 strain was β-oxidation and not *de novo* fatty acid synthesis, as was expected by design.

Complex regulatory constraints limit the PHA production from the *de novo* fatty acid synthesis pathway

The above results strongly argued in favor of potential regulatory constraints avoiding the synthesis of PHA via the *de novo* fatty acid synthesis pathway. To check the feasibility of this hypothesis, we monitored the transcription levels of the *phaF* gene as representative of the *pha* cluster in KT2440 and MM16 strains under balanced conditions using either 4HBz, 4HBz supplemented with small amounts of octanoate, or only octanoate as a control condition (Figure 5C). Since MM16 does not grow in fatty acids due to its multiple deletions in the glyoxylate shunt (Figure 4), the expression of the *phaF* gene using octanoate was monitored only in the control wild-type strain. Completing the analysis, we monitored the expression levels of *phaG*, which encodes for the (*R*)-3-hydroxydecanoyl-acyl carrier protein (ACP):CoA transacylase, the key enzyme connecting fatty acid biosynthesis and PHA production (Figure 5).

We found that *phaF* was expressed in all the analyzed strains, suggesting that *pha* genes are transcribed even in the absence of nitrogen limitation. Remarkably, higher expression levels were found growing at the expense of octanoate (Figure 5C), indicating that the presence of PHA-related carbon sources promotes the expression of genes related to the production of PHA. We also noticed only a negligible expression of *phaG* in both strains, irrespective of the carbon source used (Figure 5C). Altogether, these findings were in agreement with previous observations regarding the carbon-source-dependent induction of the *pha* genes[44] and the need for a nitrogen limitation to optimally induce the expression of *phaG* under non-fatty acid growth conditions (i.e., glucose).[45] Therefore, these results could explain, to a great extent, the preponderance of the β-oxidation pathway as a source of PHA precursors in the MM16 strain (Table S6).

Rational construction of a second-generation PHA-overproducer *P. putida* strain

Growth-coupled designs often require evolutionary engineering approaches to match the *in-silico*-predicted phenotypes and to deal with the rising regulatory constraints not taken into consideration by the GEMs.[8] In this context, the combination of rational growth-coupled designs followed by adaptive laboratory evolution (ALE) experiments has been shown to be a powerful approach in bioengineering.[7,46,47] Despite ALE advantages, we reasoned that such an approach would be very compromised in our conditions. Firstly, the inability to completely eliminate isocitrate dehydrogenase is likely limiting the strength of our growth-coupling design, which could result in evolved strains fully bypassing the production of PHA as a requirement for growth. Secondly, the inherent nature of PHA as an intracellular metabolite that accumulates in granules could potentially counter select the evolved PHA-overproducer strains since the optimal condition for PHA production favors large cell size rather than fast-growing strains. Therefore, we addressed a complete rational strategy for removing the regulatory constraints including (1) the deletion of the whole *pha* cluster, (2) the expression of a synthetic PHA operon, and (3) the rerouting of the carbon flux toward the *de novo* fatty acid biosynthesis pathway (Figure 4).

To construct the second generation of strains, we first deleted the whole *pha* cluster from MM16, yielding the MM19 strain. In a second step, we addressed the expression of the minimal set of genes required for optimal PHA production from PHA-unrelated carbon sources (i.e., 4HBz) (Figure 4). Thus, by using one-pot modular cloning, we overexpressed, under the control of the constitutive medium-strength promoter SynPro16, the *phaC1* synthase (PP_5003) required for PHA synthesis and the phasin *phaF* (PP_5007) needed for proper granule formation and stabilization. Additionally, we promoted the *de novo* fatty acid pathway by overexpressing in the same plasmid the genes *phaG* (PP_1408) and the medium-chain fatty acid-CoA ligase encoded by the gene *alkK* (PP_0763). The final plasmid (pMM55) was transferred to MM19, resulting in the strain MM19 (pMM55). As a control strain, the PP05_01 strain was used, which lacks the *pha* cluster over a wild-type background[20,48] harboring the plasmid pMM55 (Figure 4).

The performances of MM19 (pMM55) and PP05_01 (pMM55) were further evaluated and compared with those from the wild-type KT2440, MM16, and the corresponding parental PP05_01 and MM19 strains, respectively (Figures 6A and 6B). As expected due to the lack of a native *pha* cluster, the PP05_01 and MM19 strains resulted in no PHA production under balanced conditions using 3 mM octanoate and 5 mM 4HBz (C/N = 2 mol/mol). In contrast, PP05_01 (pMM55) and MM19 (pMM55) strains yielded 26% and 46% PHA/CDW, respectively (Figure 6A). Furthermore, we observed a more homogeneous population, in terms of PHA granule size and distribution among the cells, in MM19 (pMM55) compared to PP05_01 (pMM55) (Figure 6B). These findings underscore the importance of our growth-coupled design. Despite its probable incompleteness stemming from the inability to fully delete isocitrate dehydrogenase, our approach resulted in a 2-fold increase in PHA production compared to the control strain lacking the growth-coupled strategy (Figure 6A). Notably, the PHA production of MM19 (pMM55) was higher compared to the first-generation strain, MM16 (46% vs. 34% PHA/CDW). This observation would suggest that an increased PHA fraction in MM19 (pMM55) derived from the *de novo* fatty acid biosynthesis was promoted by the removal of regulatory constraints and the overexpression of *phaG* and *alkK* genes. To validate this hypothesis, we look at the monomeric composition of the resulting polymers, and a noteworthy aspect was the higher amounts of C10 monomer observed in MM19 (pMM55) (15.40%) and PP05_01 (pMM55) (9.79%) background strains compared to MM16 (1.42%) and KT2440 (4.01%) strains (Figure 6B). Taken together, these results fully validated the functionality of the synthetic operon since it led to an increased flux through the *de novo* fatty acid PHA pathway.

Upcycling PET hydrolysates into PHA using *P. putida* cells

After confirming the functionality of MM19 (pMM55) and PP05_01 (pMM55) strains, we proceeded to evaluate their performances in a practical PET upcycling scenario using PET hydrolysate and associated substrates. To enable growth on the primary PET monomers, namely EG and TPA, we constructed a series of new strains. On the one hand, EG metabolism was engineered by deleting the GntR family transcriptional regulator *gclR* (PP_4283)[49] in the MM19 and PP05_01 strains. This resulted in the creation of MM20 and PP05_18 strains, respectively. On the other hand, TPA-degrading strains were constructed by expressing the *tph* operon from *Pseudomonas umsongensis* GO16, which is included in the pBT'T plasmid. This plasmid confers the capability to efficiently use TPA in engineered *P. putida* KT2440 strains.[50] Subsequently, for PHA production assays, we subcloned into the pBT'T_ plasmid[50] the *pha*-optimized genes from pMM55 via NotI, generating the pRK190 plasmid (Figure 4).

The resulting MM20 (pRK190) and PP05_18 (pRK190) strains acquired the ability to use TPA and EG as sole carbon sources. Afterward, they were evaluated for PHA production using both an equimolar mixture of TPA and EG (20 mM) and enzymatically hydrolyzed PET without nitrogen limitation (please refer to the STAR Methods for more details; Figure 6C; Table S5). Remarkably, the putative growth-coupled strain exhibited superior performance in this scenario as well. In fact, after 50 h of growth with the synthetic TPA/EG mixture, MM20 (pRK190) achieved up to 12.38% PHA/CDW, surpassing the 8.37% PHA/CDW achieved by the control PP05_18 (pRK190) strain. Under these conditions, EG was fully consumed after 24 h by both strains; however, there remained 4 and 1 mM TPA for PP05_18 (pRK190) and MM20 (pRK190) strains, respectively.

The utilization of enzymatic PET hydrolysates does not significantly alter the trends observed thus far, with similar yields found—11.06% and 7.14% PHA/CDW produced by MM20 (pRK190) and PP05_18 (pRK190) after 50 h, respectively (Figure 6C; Table S5). As anticipated, in all the conditions tested, the monomeric PHA composition followed the *de novo* fatty acid synthesis (Figure 6C). However, a slight decrease in growth performance was noted in both strains, likely attributed to the high phosphate content of the PET hydrolysate (Table S5). We would like to emphasize that, likely owing to some hydrolysate

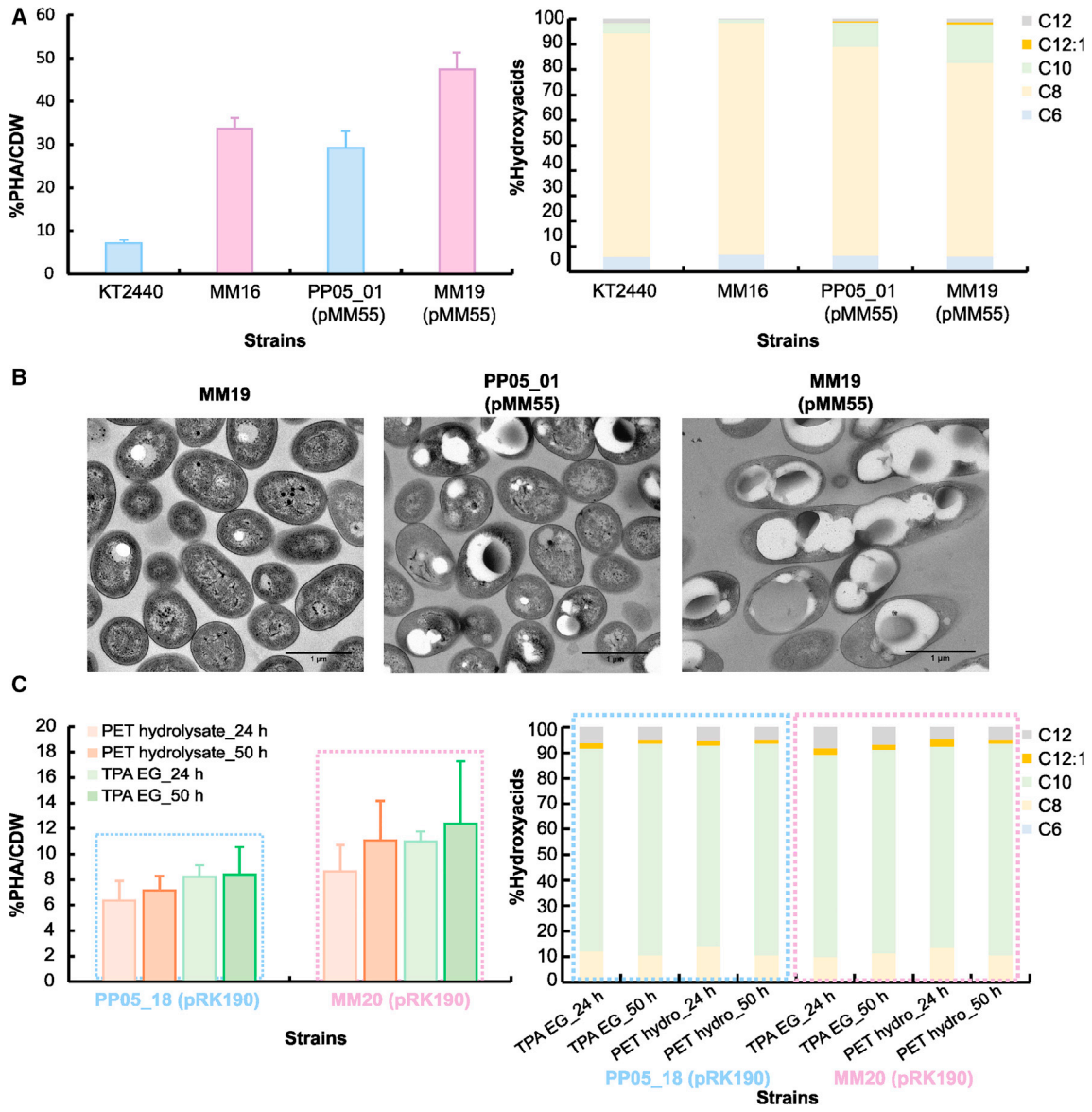


Figure 6. Phenotypic evaluation of the second-generation PHA-overproducer strains

(A) PHA production properties (i.e., %PHA/CDW and the monomeric %hydroxyacid composition) under 24 h using M63 minimal medium supplemented with 4HBz-octa (C/N ratio: 2 mol/mol).

(B) Electronic microscopy pictures of the second-generation strains grown under the abovementioned conditions. The scale bar of the pictures represents 1 μm.

(C) PHA production properties using Delft minimal medium supplemented with 20 mM TPA and 20 mM EG or PET hydrolysate, respectively, and grown over 24 and 50 h under balanced conditions.

The data of (A) and (C) correspond to the mean values and standard deviations of three independent biological replicates with two technical replicates for the methanolysis process.

variability among the biological replicates, we observed variable behavior regarding the consumption of TPA and EG among the strains. Notably, after 50 h of growth, both strains retained 14–18 mM TPA, while one replicate of MM20 (pRK190) retained 19 mM EG, in contrast to PP05_18 (pRK190), which completely consumed EG in all cases. These findings suggest that there is a significant potential for improvement not only in terms of metabolic rerouting in the producer strains but also in the context of feedstock provision.

PET4 design exhibited superior PHA overproduction abilities over a large array of carbon sources under balanced conditions

In order to expand the applicability of the PET4 growth-coupled design as a chassis for PHA production using alternative carbon sources, we conducted an *in silico* assessment of its feasibility. Specifically, we evaluated the potential of the PET4/complete design to overproduce PHA using the set of carbon sources that support *i*JNP4SB growth. As expected,

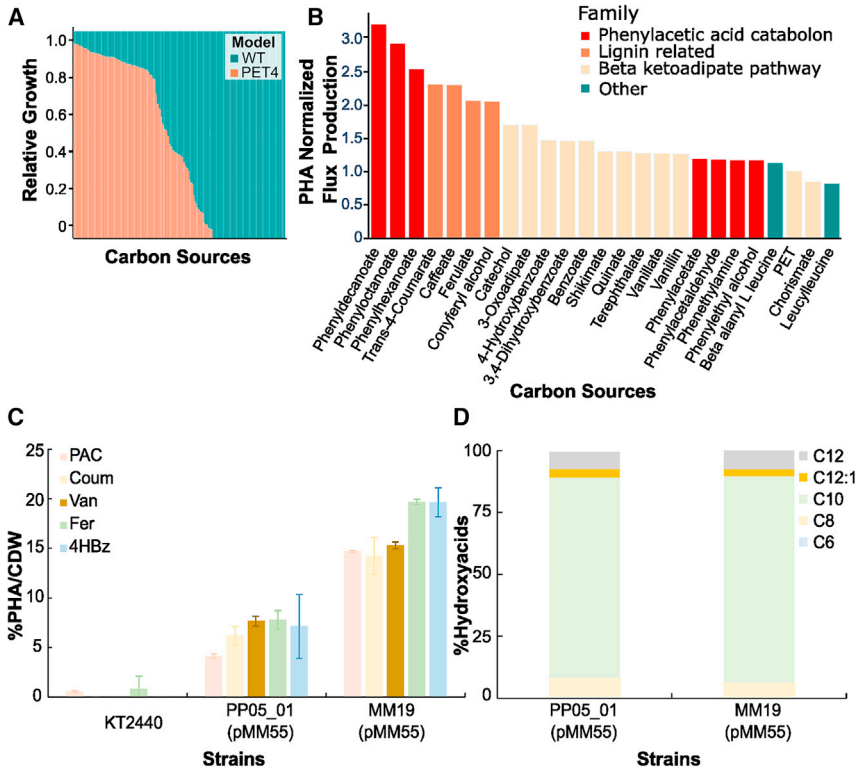


Figure 7. Strain phenotypic evaluation on different carbon sources

(A) The *in silico* growth performance of PET4 strain (depicted in orange) compared to the WT (shown in blue) strain on 210 carbon sources is shown.

(B) The PHA yield was normalized to the flux production from PET for each substrate used in this analysis. From the carbon sources supporting PET4 growth, only a few allowed growth-coupled PHA production. From these, phenylacetic acid catabolism-like compounds (red) are the most promising carbon sources. The lignin related (in orange), β-ketoadipate pathway derived (in light yellow), and other derivatives (in blue) are shown. The uptake rate for all the carbon sources was 5 mmol gDW^{-1} h^{-1}.

(C) Experimental validation of PHA production under different carbon sources: 4.4 mM phenylacetic acid (PAC; light pink color), 3.9 mM p-coumaric acid (Coum; light yellow color), 4.4 mM vanillic acid (Van; brown color), 3.5 mM ferulic acid (Fer; light green color), and 5 mM 4HBz (light blue color). The data correspond to the mean values and standard deviations of two independent biological replicates with two technical replicates for the methanolysis process except PAC, which corresponds to one biological replicate.

(D) %Hydroxyacid monomeric composition under 24 h of growth using M63 minimal medium supplemented with 5 mM 4HBz (C/N ratio: 2 mol/mol).

the *in silico* PET4 strain exhibited a reduced metabolic versatility compared to the wild-type model due to the large number of gene deletions introduced (Figure 7A). For example, the deletion of the glyoxylate shunt prevented the growth of PET4 on fatty acids as carbon sources. Nevertheless, it was noteworthy that from the carbon sources supporting growth, a significant fraction of them, the majority being aromatic compounds, allowed *in silico* growth-coupled PHA production (Figure 7B). Overall, the most promising carbon sources as feedstock for PHA production were metabolites catabolized via acetyl-CoA and succinate/succinyl-CoA,[51] for instance metabolites belonging to (1) the phenylacetyl-CoA catabolome,[52] (2) lignin-related carbon sources such as phenylpropanoids, and (3) other aromatic compounds catabolized via the β-ketoadipate pathway. Subsequently, we tested whether MM19 (pMM55) and PP05_01 (pMM55) could overproduce PHA using selected aromatic compounds as the sole carbon source in the absence of PHA-related co-substrates (i.e., octanoic acid) and nitrogen limitation.

Agreeing with the model predictions, while the wild-type strain was unable to accumulate PHA using 4HBz as a sole carbon source, the recombinant strains did. Indeed, the PP05_01 (pMM55) strain, in which the regulatory constraints hampering PHA production were removed while harboring the pMM55 plasmid, resulted in more than 5% PHA/CDW (Figure 7C). Notably, emphasizing again the synergistic effect of the growth-coupled designs and the removal of regulatory constraints, the MM19 (pMM55) strain accumulated up to 17.65% PHA/CDW (Figure 7C). As expected, the PHA monomeric compositions in both strains showed profiles compatible with the use of the *de novo* fatty acid pathway, with C10 monomers representing more than 80% (Figure 7D).

We further explored the suitability of other recalcitrant carbon sources derived from the hydrolysis of complex polymers (i.e., coumarate, ferulate, vanillate, phenylacetic acid). As expected, the wild-type strain produced only negligible amounts of PHA when using p-coumarate, ferulate, or vanillate as the carbon source. However, the PP05_01 (pMM55) strain exhibited PHA accumulation ranging from 4% to 8% of the total biomass (Figure 7C). The MM19 (pMM55) strain produced significantly higher amounts of PHA reaching up to 19.68% PHA/CDW using ferulate as the sole carbon source. Furthermore, we continued by testing the PHA production using phenylacetate since it was proposed as a promising carbon source for PHA production by providing up to 2 acetyl-CoA molecules. Once more, validating the *in silico* predictions, the MM19 (pMM55) strain was able to produce up to 14.7% of PHA/CDW after 72 h of cultivation compared to the negligible amounts produced by the wild-type strain (Figure 7C).

In summary, we presented a collection of PHA-overproducer mutant strains able to produce PHA under balanced growth conditions in terms of C/N ratio by using a variety of recalcitrant carbon sources as the sole carbon and energy sources. The growth-coupled designs, even likely incomplete *in vivo*, proved to be a critical tool for rerouting the carbon flux toward PHA production by using the PCA as a key metabolic hub.

DISCUSSION

In the last years, there has been increasing interest in PET upcycling and plastics revalorization into higher-value-added products. In this context, substantial efforts have been directed toward enhancing the enzymes involved in the polymer degradation such as PETases, cutinases, etc.[53–55] However, it is surprising that a significantly smaller workforce has been dedicated to the further revalorization of enzymatic hydrolysates.[56,57] Here, we faced the demanding transformation of recalcitrant monomeric constituents derived from the hydrolysis of complex polymers (i.e., PET, lignin) into bioplastics, PHAs.

Growth-coupling overproducing approach is a valuable strategy even at reduced coupling strength

In the new era of synthetic metabolism, metabolic fluxes can be rewired by employing rationally designed selection strains in the context of well-structured DBTL cycles as an alternative to traditional metabolic engineering strategies.[8] However, this large cell refactoring usually places a burden on the organism often resulting in reduced growth performance. In this way, without coupling the functionality that is needed for production during the bacterium's growth, the implemented synthetic function could be lost from a production strain, which adapts to a higher growth rate at this functionality.[9,58] In fact, growth coupling is a highly desirable trait, as (1) it minimizes the effect of undesirable regulatory constraints, (2) alleviates the genetic instability and selection problems that can result from classical metabolic engineering, and (3) enables the use of ALE to further increase the production rate.[59]

Here, we *in silico* evaluated the PHA growth-coupling landscape of *P. putida* using computational approaches and *in vivo* implemented one of the most promising designs. Nevertheless, we faced several challenges to completing this *in vivo* validation. Initially, the challenge of fully deleting isocitrate dehydrogenase likely restricted the efficacy of our growth-coupling strain. Additionally, the intrinsic nature of PHA, acting as an intracellular metabolite accumulating in granules, could pose a counterselection pressure on evolved PHA-overproducer strains. Taken together, these limitations hindered the utilization of ALE experiments to enhance the growth coupling of PHA production. Consequently, our constructed strain likely displays a weak growth-coupling phenotype. Furthermore, we cannot rule out the possibility that the MM16 strain exhibits a non-growth-coupled phenotype similar to that shown in the minimal PET4 design (Figure 3D). This hypothesis gained support from the absence of observed growth deficiencies in this strain in the absence of PHA accumulation.

Nevertheless, we significantly overcame this limitation by rationally constructing second-generation strains that lacked the regulatory constraints responsible for the poor performance of PHA production using precursors derived from the *de novo* fatty acid biosynthesis pathway. The new strains demonstrated superior PHA production rates not only by co-feeding with PHA-related carbon source (e.g., octanoate) but also at the expense of unrelated feedstocks as the sole carbon source. An increased flux was also observed through the *de novo* fatty acid synthesis pathway. More importantly, the advantage of the growth-coupled metabolic background was thoroughly demonstrated, despite its incompleteness and/or reduced coupling strength. For instance, the MM16 strain, harboring the growth-coupled intermediate design, accumulated significantly higher PHA than the wild-type strain using 4HBz and octanoate—33.70% (0.2 g/L) compared to 7.09% PHA/CDW (0.05 g/L). Additionally, the second generation of growth-coupled strains (MM19 and MM20) harboring either pMM55 or pRK190 significantly surpassed the production of their counterpart strains lacking the design (PP05_01 and PP05_18) using also unrelated carbon sources and in the absence of nitrogen limitation (Figures 5 and 6). Notably, we observed that the mere elimination of regulatory constraints in the PP05_01 (pMM55) strain proved to be an effective approach to overcome nutrient limitation for PHA production. However, our findings demonstrated that achieving optimal PHA production required the synergistic effect of regulatory removal and carbon flux rerouting, as exemplified by the MM19 (pMM55) strain.

Overall, we have demonstrated to a great extent that our engineered strains (1) exhibit improved PHA production capability, (2) overcome nutrient limitations for PHA production, and (3) harbor carbon flux rerouting based on a growth-coupling design that yields superior PHA production.

Improving PET upcycling with *P. putida* KT2440

The enzymatic degradation of PET to enhance its biodegradability has been an ongoing and prominent topic capturing the attention of a significant workforce in the last decade.[54,55] However, the upcycling of the subsequent PET hydrolysates using microbial factories have been addressed only very recently. In a valuable pioneer work, bioupcycling of PET was addressed using *P. umsongensis* GO16.[57] This strain is a natural TPA-degrader strain, and it was engineered to further use EG. The resulting strain was able to efficiently co-utilize EG and TPA and convert them into mcl-PHA. The main drawback of this promising work was the low PHA yields obtained: approximately 7% PHA/CDW by applying the conventional nitrogen-limited conditions.[57] By dual engineering of EG and TPA metabolisms within the framework of a growth-coupled design, we demonstrated here that the *P. putida* MM20 (pRK190) strain is a great candidate for further implementation in plastic revalorization strategies. In fact, this strain reached up to 12.5% of PHA/CDW (0.10–0.17 g/L) using a synthetic mixture of TPA and EG or PET hydrolysate without nitrogen limitation. Therefore, as indicated by the growth deficiencies observed in the context of PET hydrolysate upcycling, there is still a substantial opportunity for improvement in both strain design and feedstock supply.

Expanding the scope of PHA-overproducer strains toward recalcitrant feedstocks

Taking advantage of the metabolic funneling concept, in this work, we further expanded the applicability of our engineered strain toward the upcycling of a range of aromatic compounds, including lignin-related carbon sources (Figure 7; Table S5).

Lignin and lignin-related compounds have already been explored as suitable feedstocks for PHA production through increasing levels of engineering in *Pseudomonas* strains (Table S7).[36,60–64] In this vein, Salvachúa and collaborators

demonstrated the efficiency of combining synthetic biology/metabolic engineering strategies and optimizing culture growth conditions to improve PHA yields from key lignin-related components.[65] Specifically, fed-batch cultures of the engineered *P. putida* KT2440 strain combined with high cell densities reached up to 0.95 g/L PHA production after 85 h of growth. Despite this high yield, such large cell refactoring was unable to uncouple PHA production from nitrogen limitation, and nitrogen-limited conditions (C/N ratio: 55.6 mol/mol; Table S7) were required for production.[65] Notably, a recent attempt to decouple PHA from nitrogen limitation has been successful using the non-model *P. putida* A514 strain. In this study, a library of engineered *P. putida* A514 strains overexpressing the PHA pathway using different inducible expression systems was constructed. When the library was tested for PHA production at different C/N ratios supplemented with 15 mM vanillic acid (high: 98.4 mol/mol and low: 6.5 mol/mol), productions of up to 34.4% were reported.[66,67] Remarkably, nitrogen limitation could be overcome due to the fact that the key genes involved in the *de novo* biosynthesis pathway (i.e., including 3-hydroxyacyl-ACP thioesterase [*phaG*] and long-chain fatty acid-CoA ligase [*alkK*]) were significantly expressed under both high and low nitrogen (N) conditions, contrary to what occurs in the KT2440 strain. Therefore, the optimal combination described by the engineered strain of *P. putida* A514 resembles that of the PP05_01 (pMM55) strain, where the intrinsic regulatory constraints were synthetically removed. Notably, in our case, PHA production was achieved at a significantly lower C/N ratio scenario (1.12 mol/mol using 4.4 mM vanillic acid). Therefore, with the construction of MM19 (pMM55) and MM20 (pRK190) strains, we take a significant step forward by additionally rerouting central metabolism toward PHA production. An interesting question that arises is whether the implementation of a similar growth-coupling design in *P. putida* A514 could increase PHA production in this strain at a similar rate to *P. putida* KT2440. If so, the resulting strain would definitely be of great industrial value.

Limitations of the study

Here, we take a valuable step forward toward the long-term goal of the cost-effective conversion of recalcitrant polymers into sustainable and more degradable bioplastics. Notably, it is important to emphasize that, in pursuit of this ambitious objective, we faced both foreseen and unforeseen challenges.

Firstly, several limitations encountered relied on the feasibility of the accurate *in vivo* implementation of model-driven designs. Our study highlights intrinsic limitations, such as the nature of PHA, which complicates ALE experiments, as well as the unknown effects on cell viability due to deleting IDH, as the main reasons preventing the successful construction of overproducing strains exhibiting high-strength growth coupling. However, we cannot discard additional unknown effects derived from the high number of genetic modifications and/or metabolic knowledge missing in the GEM of *P. putida* as additional sources of this infeasibility. Taken together, our data verify that the lack of metabolic/physiological knowledge regarding the microbial cell factory is still an important limitation in rational bioengineering. Therefore, efforts toward the system-level understanding of overproducer strains, such as that we present here, becomes of high value for the community.

Secondly, we have realized that raw material supply, often underestimated, is not a trivial issue when it comes to recalcitrant compounds. PET hydrolysates were generated using a very high buffer capacity, therefore providing challenging growth conditions for *P. putida* and thus contributing to decreased growth and PHA production performance. Similar behavior was observed when using lignin hydrolysates, which implies that it is a common limitation in polymer upcycling and needs to be taken into account. Whether the use of more friendly polymer pre-processing steps and/or the use/engineering of more robust microbial hosts could successfully address this limitation is something that needs to be explored in the near future.

STAR★METHODS

Detailed methods are provided in the online version of this paper and include the following:

- KEY RESOURCES TABLE
- RESOURCE AVAILABILITY
  - Lead contact
  - Materials availability
  - Data and code availability
- EXPERIMENTAL MODEL AND STUDY PARTICIPANT DETAILS
  - Bacterial strains, media and culture conditions
- METHOD DETAILS
  - Physiological studies and parameters calculation
  - Construction of *P. putida* engineered strains
  - Golden gate/MoClo plasmid construction
  - RNA extraction and real-time qPCR experiments
  - PHA determination by methanolysis and GC-MS analysis
  - TPA quantification using HPLC-MS
  - Extracellular metabolites identification by HPLC
  - Microscopy assays
  - Constraint-based flux analysis
  - Model-driven design of growth-coupled PHA strains
  - *In silico* manual curation for candidate's selection
- QUANTIFICATION AND STATISTICAL ANALYSIS

SUPPLEMENTAL INFORMATION

Supplemental information can be found online at https://doi.org/10.1016/j.celrep.2024.113979.

ACKNOWLEDGMENTS

The authors thank Lars Blank and Gina Welsing for providing the PET hydrolysate substrate for PET upcycling assays. We also thank Tanja Narancic and Kevin O'Connor for providing the pBT'T_*tph* plasmid for TPA degradation assays. We acknowledge Ryan Kniewel and Sergio Salgado for the construction of some of the plasmids used in this study and David San Leon for helping with Figures 2 and 5. Ana Valencia's technical work is also greatly appreciated. Finally, we thank the Spanish National Research Council (CSIC) and the Margarita Salas Centre for Biological Research (CIB-CSIC) for its scientific support and the use of its facilities. This research received funding from the European Union's Horizon 2020 research and innovation program under grant agreement nos. 633962 (P4SB), 870294 (MIX-up), and 101000733 (PROMICON). We also acknowledge support from the Spanish Ministry of Innovation and Science (AEI/10.13039/501100011033) through projects

BIO2017-83448-R_TECMABIO, PID2020-112766RB-C21-BIOCIR, PID2022-139247OB-I00 (Rob3D), and TED2021-130689B-C33 (SyCoSys). Funding was likewise provided by CSIC's Interdisciplinary Platform for Sustainable Plastics toward a Circular Economy+ (PTI-SusPlast+).

AUTHOR CONTRIBUTIONS

J.N. and M.A.P. conceived the study and the experimental approach and handled funding acquisition, supervision, and writing – review & editing. M.-T.M. performed and designed the experimental procedures and wrote the original draft. M.-T.M., A.G.-B., C.d.C.S., and J.N. performed and analyzed the *in silico* analyses and growth-coupled model generation. V.R.-B. designed the analytical protocols of high-performance liquid chromatography and gas chromatography-mass spectrometry assays. All authors analyzed and discussed the results and wrote the manuscript.

DECLARATION OF INTERESTS

From this work, a patent application was registered.

Received: August 9, 2023
Revised: January 29, 2024
Accepted: March 6, 2024
Published: March 22, 2024

REFERENCES

1. Nielsen, J., and Keasling, J.D. (2016). Engineering Cellular Metabolism. Cell *164*, 1185–1197. https://doi.org/10.1016/j.cell.2016.02.004.
2. Opgenorth, P., Costello, Z., Okada, T., Goyal, G., Chen, Y., Gin, J., Benites, V., de Raad, M., Northen, T.R., Deng, K., et al. (2019). Lessons from Two Design–Build–Test–Learn Cycles of Dodecanol Production in *Escherichia coli* Aided by Machine Learning. ACS Synth. Biol. *8*, 1337–1351. https://doi.org/10.1021/acssynbio.9b00020.
3. Gurdo, N., Volke, D.C., McCloskey, D., and Nikel, P.I. (2023). Automating the design-build-test-learn cycle towards next-generation bacterial cell factories. N. Biotech. *74*, 1–15, S187167842300002X. https://doi.org/10.1016/j.nbt.2023.01.002.
4. Noh, M.H., Cha, S., Kim, M., and Jung, G.Y. (2020). Recent Advances in Microbial Cell Growth Regulation Strategies for Metabolic Engineering. Biotechnol Bioproc E *25*, 810–828. https://doi.org/10.1007/s12257-019-0511-x.
5. Gudmundsson, S., and Nogales, J. (2021). Recent advances in model-assisted metabolic engineering. Curr. Opin. Struct. Biol. *28*, 100392. https://doi.org/10.1016/j.coisb.2021.100392.
6. Hoek, M.J.A.v., and Merks, R.M.H. (2017). Emergence of microbial diversity due to cross-feeding interactions in a spatial model of gut microbial metabolism. BMC Syst. Biol. *11*, 56. https://doi.org/10.1186/s12918-017-0430-4.
7. Konstantinidis, D., Pereira, F., Geissen, E.M., Grkovska, K., Kafkia, E., Jouhten, P., Kim, Y., Devendran, S., Zimmermann, M., and Patil, K.R. (2021). Adaptive laboratory evolution of microbial co-cultures for improved metabolite secretion. Mol. Syst. Biol. *17*, e10189. https://doi.org/10.15252/msb.202010189.
8. Orsi, E., Claassens, N.J., Nikel, P.I., and Lindner, S.N. (2021). Growth-coupled selection of synthetic modules to accelerate cell factory development. Nat. Commun. *12*, 5295. https://doi.org/10.1038/s41467-021-25665-6.
9. von Kamp, A., and Klamt, S. (2017). Growth-coupled overproduction is feasible for almost all metabolites in five major production organisms. Nat. Commun. *8*, 15956. https://doi.org/10.1038/ncomms15956.
10. King, Z.A., O'Brien, E.J., Feist, A.M., and Palsson, B.O. (2017). Literature mining supports a next-generation modeling approach to predict cellular byproduct secretion. Metab. Eng. *39*, 220–227. https://doi.org/10.1016/j.ymben.2016.12.004.
11. Fong, S.S., Burgard, A.P., Herring, C.D., Knight, E.M., Blattner, F.R., Maranas, C.D., and Palsson, B.O. (2005). In silico design and adaptive evolution of *Escherichia coli* for production of lactic acid. Biotechnol. Bioeng. *91*, 643–648. https://doi.org/10.1002/bit.20542.
12. Trinh, C.T., and Srienc, F. (2009). Metabolic Engineering of *Escherichia coli* for Efficient Conversion of Glycerol to Ethanol. Appl. Environ. Microbiol. *75*, 6696–6705. https://doi.org/10.1128/AEM.00670-09.
13. Xu, P., Ranganathan, S., Fowler, Z.L., Maranas, C.D., and Koffas, M.A.G. (2011). Genome-scale metabolic network modeling results in minimal interventions that cooperatively force carbon flux towards malonyl-CoA. Metab. Eng. *13*, 578–587. https://doi.org/10.1016/j.ymben.2011.06.008.
14. Harder, B.-J., Bettenbrock, K., and Klamt, S. (2016). Model-based metabolic engineering enables high yield itaconic acid production by *Escherichia coli*. Metab. Eng. *38*, 29–37. https://doi.org/10.1016/j.ymben.2016.05.008.
15. Manoli, M.T., Tarazona, N., Mato, A., Maestro, B., Sanz, J.M., Nogales, J., and Prieto, M.A. (2020). Molecular Basis of Medium-Chain Length-PHA Metabolism of Pseudomonas putida. In The Handbook of Polyhydroxyalkanoates (CRC Press), pp. 89–114.
16. Mezzina, M.P., Manoli, M.T., Prieto, M.A., and Nikel, P.I. (2021). Engineering native and synthetic pathways in *Pseudomonas putida* for the production of tailored polyhydroxyalkanoates. Biotechnol. J. *16*, 2000165.
17. De Eugenio, L.I., Escapa, I.F., Morales, V., Dinjaski, N., Galán, B., García, J.L., and Prieto, M.A. (2010). The turnover of medium-chain-length polyhydroxyalkanoates in Pseudomonas putida KT2442 and the fundamental role of PhaZ depolymerase for the metabolic balance. Environ. Microbiol. *12*, 207–221. https://doi.org/10.1111/j.1462-2920.2009.02061.x.
18. Prieto, A., Escapa, I.F., Martínez, V., Dinjaski, N., Herencias, C., de la Peña, F., Tarazona, N., and Revelles, O. (2016). A holistic view of polyhydroxyalkanoate metabolism in *Pseudomonas putida*. Environ. Microbiol. *18*, 341–357. https://doi.org/10.1111/1462-2920.12760.
19. Tarazona, N.A., Maestro, B., Revelles, O., Sanz, J.M., and Prieto, M.A. (2019). Role of leucine zipper-like motifs in the oligomerization of *Pseudomonas putida* phasins. Biochim. Biophys. Acta Gen. Subj. *1863*, 362–370. https://doi.org/10.1016/j.bbagen.2018.11.002.
20. Manoli, M.-T., Nogales, J., and Prieto, A. (2022). Synthetic Control of Metabolic States in Pseudomonas putida by Tuning Polyhydroxyalkanoate Cycle. mBio, e017944-e1821. https://doi.org/10.1128/mbio.01794-21.
21. Ruiz, C., Kenny, S.T., Narancic, T., Babu, R., and Connor, K.O. (2019). Conversion of waste cooking oil into medium chain polyhydroxyalkanoates in a high cell density fermentation. J. Biotechnol. *306*, 9–15. https://doi.org/10.1016/j.jbiotec.2019.08.020.
22. Zheng, Y., Chen, J.-C., Ma, Y.-M., and Chen, G.-Q. (2020). Engineering biosynthesis of polyhydroxyalkanoates (PHA) for diversity and cost reduction. Metab. Eng. *58*, 82–93. https://doi.org/10.1016/j.ymben.2019.07.004.
23. Palleroni, N.J. (2010). The Pseudomonas Story: Editorial. Environ. Microbiol. *12*, 1377–1383. https://doi.org/10.1111/j.1462-2920.2009.02041.x.
24. Kampers, L.F.C., Volkers, R.J.M., and Martins dos Santos, V.A.P. (2019). *Pseudomonas putida* KT 2440 is HV 1 certified, not GRAS. Microb. Biotechnol. *12*, 845–848. https://doi.org/10.1111/1751-7915.13443.
25. Nikel, P.I., Chavarría, M., Danchin, A., and de Lorenzo, V. (2016). From dirt to industrial applications: Pseudomonas putida as a Synthetic Biology chassis for hosting harsh biochemical reactions. https://doi.org/10.1016/j.cbpa.2016.05.011.
26. Nogales, J., Mueller, J., Gudmundsson, S., Canalejo, F.J., Duque, E., Monk, J., Feist, A.M., Ramos, J.L., Niu, W., and Palsson, B.O. (2020). High-quality genome-scale metabolic modelling of *Pseudomonas putida*

highlights its broad metabolic capabilities. Environ. Microbiol. *22*, 255–269. https://doi.org/10.1111/1462-2920.14843.

27. Liu, S., Narancic, T., Tham, J.-L., and O'Connor, K.E. (2023). β-oxidation–polyhydroxyalkanoates synthesis relationship in *Pseudomonas putida* KT2440 revisited. Appl. Microbiol. Biotechnol. *107*, 1863–1874. https://doi.org/10.1007/s00253-023-12413-7.
28. Guzik, M.W., Narancic, T., Ilic-Tomic, T., Vojnovic, S., Kenny, S.T., Casey, W.T., Duane, G.F., Casey, E., Woods, T., Babu, R.P., et al. (2014). Identification and characterization of an acyl-CoA dehydrogenase from *Pseudomonas putida* KT2440 that shows preference towards medium to long chain length fatty acids. Microbiol. *160*, 1760–1771. https://doi.org/10.1099/mic.0.078758-0.
29. Andin, N., Longieras, A., Veronese, T., Marcato, F., Molina-Jouve, C., and Uribelarrea, J.-L. (2017). Improving carbon and energy distribution by coupling growth and medium chain length polyhydroxyalkanoate production from fatty acids by *Pseudomonas putida* KT2440. Biotechnol Bioproc E *22*, 308–318. https://doi.org/10.1007/s12257-016-0449-1.
30. Escapa, I.F., del Cerro, C., García, J.L., and Prieto, M.A. (2013). The role of GlpR repressor in *Pseudomonas putida* KT2440 growth and PHA production from glycerol: *Pseudomonas putida* growth and PHA production from glycerol. Environ. Microbiol. *15*, 93–110. https://doi.org/10.1111/j.1462-2920.2012.02790.x.
31. Borrero-de Acuña, J.M., Bielecka, A., Häussler, S., Schobert, M., Jahn, M., Wittmann, C., Jahn, D., and Poblete-Castro, I. (2014). Production of medium chain length polyhydroxyalkanoate in metabolic flux optimized *Pseudomonas putida*. Microb. Cell Factories *13*, 88. https://doi.org/10.1186/1475-2859-13-88.
32. Danso, D., Chow, J., and Streit, W.R. (2019). Plastics: Environmental and Biotechnological Perspectives on Microbial Degradation. Appl. Environ. Microbiol. *85*, e010955-e1119,/aem/85/19/AEM.01095-19.atom. https://doi.org/10.1128/AEM.01095-19.
33. Tiso, T., Winter, B., Wei, R., Hee, J., De Witt, J., Wierckx, N., Quicker, P., Bornscheuer, U.T., Bardow, A., Nogales, J., and Blank, L.M. (2022). The metabolic potential of plastics as biotechnological carbon sources – Review and targets for the future. Metab. Eng. *71*, 77–98. https://doi.org/10.1016/j.ymben.2021.12.006.
34. Nogales, J., García, J.L., and Díaz, E. (2017). Degradation of Aromatic Compounds in Pseudomonas: A Systems Biology View. In Aerobic Utilization of Hydrocarbons, Oils and Lipids, F. Rojo, ed. (Springer International Publishing), pp. 1–49. https://doi.org/10.1007/978-3-319-39782-5_32-1.
35. Li, F., Zhao, Y., Xue, L., Ma, F., Dai, S.Y., and Xie, S. (2022). Microbial lignin valorization through depolymerization to aromatics conversion. Trends Biotechnol. *40*, 1469–1487. https://doi.org/10.1016/j.tibtech.2022.09.009.
36. Linger, J.G., Vardon, D.R., Guarnieri, M.T., Karp, E.M., Hunsinger, G.B., Franden, M.A., Johnson, C.W., Chupka, G., Strathmann, T.J., Pienkos, P.T., and Beckham, G.T. (2014). Lignin valorization through integrated biological funneling and chemical catalysis. Proc. Natl. Acad. Sci. USA *111*, 12013–12018. https://doi.org/10.1073/pnas.1410657111.
37. Ramírez-Morales, J.E., Czichowski, P., Besirlioglu, V., Regestein, L., Rabaey, K., Blank, L.M., and Rosenbaum, M.A. (2021). Lignin Aromatics to PHA Polymers: Nitrogen and Oxygen Are the Key Factors for *Pseudomonas*. ACS Sustainable Chem. Eng. *9*, 10579–10590. https://doi.org/10.1021/acssuschemeng.1c02682.
38. Nogales, J., Gudmundsson, S., Duque, E., Ramos, L., and Bernhard, O. (2017). Expanding the computable reactome in *Pseudomonas putida* reveals metabolic cycles providing robustness. https://doi.org/10.1101/139121.
39. Legon, L., Corre, C., Bates, D.G., and Mannan, A.A. (2022). gcFront: a tool for determining a Pareto front of growth-coupled cell factory designs. Bioinformatics *38*, 3657–3659. https://doi.org/10.1093/bioinformatics/btac376.
40. Wierckx, N., Narancic, T., Eberlein, C., Wei, R., Drzyzga, O., Magnin, A., Ballerstedt, H., Kenny, S.T., Pollet, E., Avérous, L., et al. (2018). Plastic Biodegradation: Challenges and Opportunities. In Consequences of Microbial Interactions with Hydrocarbons, Oils, and Lipids: Biodegradation and Bioremediation, R. Steffan, ed. (Springer International Publishing), pp. 1–29. https://doi.org/10.1007/978-3-319-44535-9_23-1.
41. Salvador, M., Abdulmutalib, U., Gonzalez, J., Kim, J., Smith, A.A., Faulon, J.-L., Wei, R., Zimmermann, W., and Jimenez, J.I. (2019). Microbial Genes for a Circular and Sustainable Bio-PET Economy. Genes *10*, 373. https://doi.org/10.3390/genes10050373.
42. Belisário-Ferrari, M.R., Wei, R., Schneider, T., Honak, A., and Zimmermann, W. (2019). Fast Turbidimetric Assay for Analyzing the Enzymatic Hydrolysis of Polyethylene Terephthalate Model Substrates. Biotechnol. J. *14*, 1800272. https://doi.org/10.1002/biot.201800272.
43. Klinke, S., Dauner, M., Scott, G., Kessler, B., and Witholt, B. (2000). Inactivation of isocitrate lyase leads to increased production of medium-chain-length poly(3-hydroxyalkanoates) in *Pseudomonas putida*. Appl. Environ. Microbiol. *66*, 909–913. https://doi.org/10.1128/AEM.66.3.909-913.2000.
44. De Eugenio, L.I., Galán, B., Escapa, I.F., Maestro, B., Sanz, J.M., García, J.L., and Prieto, M.A. (2010). The PhaD regulator controls the simultaneous expression of the pha genes involved in polyhydroxyalkanoate metabolism and turnover in *Pseudomonas putida* KT2442. Environ. Microbiol. *12*, 1591–1603. https://doi.org/10.1111/j.1462-2920.2010.02199.x.
45. Wang, Q., Tappel, R.C., Zhu, C., and Nomura, C.T. (2012). Development of a new strategy for production of medium-chain-length polyhydroxyalkanoates by recombinant *Escherichia coli* via inexpensive non-fatty acid feedstocks. Appl. Environ. Microbiol. *78*, 519–527. https://doi.org/10.1128/AEM.07020-11.
46. Jouhten, P., Konstantinidis, D., Pereira, F., Andrejev, S., Grkovska, K., Castillo, S., Ghiachi, P., Beltran, G., Almaas, E., Mas, A., et al. (2022). Predictive evolution of metabolic phenotypes using model-designed environments. Mol. Syst. Biol. *18*, e10980. https://doi.org/10.15252/msb.202210980.
47. Wu, Y., Jameel, A., Xing, X.-H., and Zhang, C. (2022). Advanced strategies and tools to facilitate and streamline microbial adaptive laboratory evolution. Trends Biotechnol. *40*, 38–59. https://doi.org/10.1016/j.tibtech.2021.04.002.
48. Mato, A., Blanco, F.G., Maestro, B., Sanz, J.M., Pérez-Gil, J., and Prieto, M.A. (2020). Dissecting the Polyhydroxyalkanoate-Binding Domain of the PhaF Phasin: Rational Design of a Minimized Affinity Tag. Appl. Environ. Microbiol. *86*, e00570-20. https://doi.org/10.1128/AEM.00570-20.
49. Franden, M.A., Jayakody, L.N., Li, W.-J., Wagner, N.J., Cleveland, N.S., Michener, W.E., Hauer, B., Blank, L.M., Wierckx, N., Klebensberger, J., and Beckham, G.T. (2018). Engineering *Pseudomonas putida* KT2440 for efficient ethylene glycol utilization. Metab. Eng. *48*, 197–207. https://doi.org/10.1016/j.ymben.2018.06.003.
50. Narancic, T., Salvador, M., Hughes, G.M., Beagan, N., Abdulmutalib, U., Kenny, S.T., Wu, H., Saccomanno, M., Um, J., O'Connor, K.E., and Jiménez, J.I. (2021). Genome analysis of the metabolically versatile *Pseudomonas umsongensis* GO16: the genetic basis for PET monomer upcycling into polyhydroxyalkanoates. Microb. Biotechnol. *14*, 2463–2480. https://doi.org/10.1111/1751-7915.13712.
51. Nogales, J., Macchi, R., Franchi, F., Barzaghi, D., Fernández, C., García, J.L., Bertoni, G., and Díaz, E. (2007). Characterization of the last step of the aerobic phenylacetic acid degradation pathway. Microbiol. *153*, 357–365. https://doi.org/10.1099/mic.0.2006/002444-0.
52. Luengo, J.M., García, J.L., and Olivera, E.R. (2001). The phenylacetyl-CoA catabolon: a complex catabolic unit with broad biotechnological applications. Mol. Microbiol. *39*, 1434–1442. https://doi.org/10.1046/j.1365-2958.2001.02344.x.

53. Liu, F., Wang, T., Yang, W., Zhang, Y., Gong, Y., Fan, X., Wang, G., Lu, Z., and Wang, J. (2023). Current advances in the structural biology and molecular engineering of PETase. Front. Bioeng. Biotechnol. *11*, 1263996. https://doi.org/10.3389/fbioe.2023.1263996.

54. Sui, B., Wang, T., Fang, J., Hou, Z., Shu, T., Lu, Z., Liu, F., and Zhu, Y. (2023). Recent advances in the biodegradation of polyethylene terephthalate with cutinase-like enzymes. Front. Microbiol. *14*, 1265139. https://doi.org/10.3389/fmicb.2023.1265139.

55. Sevilla, M.E., Garcia, M.D., Perez-Castillo, Y., Armijos-Jaramillo, V., Casado, S., Vizuete, K., Debut, A., and Cerda-Mejía, L. (2023). Degradation of PET Bottles by an Engineered *Ideonella sakaiensis* PETase. Polymers *15*, 1779. https://doi.org/10.3390/polym15071779.

56. Bao, T., Qian, Y., Xin, Y., Collins, J.J., and Lu, T. (2023). Engineering microbial division of labor for plastic upcycling. Nat. Commun. *14*, 5712. https://doi.org/10.1038/s41467-023-40777-x.

57. Tiso, T., Narancic, T., Wei, R., Pollet, E., Beagan, N., Schröder, K., Honak, A., Jiang, M., Kenny, S.T., Wierckx, N., et al. (2021). Towards bio-upcycling of polyethylene terephthalate. Metab. Eng. *66*, 167–178. https://doi.org/10.1016/j.ymben.2021.03.011.

58. Alter, T.B., and Ebert, B.E. (2019). Determination of growth-coupling strategies and their underlying principles. BMC Bioinf. *20*, 447. https://doi.org/10.1186/s12859-019-2946-7.

59. Conrad, T.M., Lewis, N.E., and Palsson, B.Ø. (2011). Microbial laboratory evolution in the era of genome-scale science. Mol. Syst. Biol. *7*, 509. https://doi.org/10.1038/msb.2011.42.

60. Tomizawa, S., Chuah, J.A., Matsumoto, K., Doi, Y., and Numata, K. (2014). Understanding the limitations in the biosynthesis of polyhydroxyalkanoate (PHA) from lignin derivatives. ACS Sustain. Chem. Eng. *2*, 1106–1113. https://doi.org/10.1021/sc500066f.

61. Salvachúa, D., Karp, E.M., Nimlos, C.T., Vardon, D.R., and Beckham, G.T. (2015). Towards lignin consolidated bioprocessing: simultaneous lignin depolymerization and product generation by bacteria. Green Chem. *17*, 4951–4967. https://doi.org/10.1039/c5gc01165e.

62. Beckham, G.T., Johnson, C.W., Karp, E.M., Salvachúa, D., and Vardon, D.R. (2016). Opportunities and challenges in biological lignin valorization. Curr. Opin. Biotechnol. *42*, 40–53. https://doi.org/10.1016/j.copbio.2016.02.030.

63. Ravi, K., García-Hidalgo, J., Gorwa-Grauslund, M.F., and Lidén, G. (2017). Conversion of lignin model compounds by *Pseudomonas putida* KT2440 and isolates from compost. Appl. Microbiol. Biotechnol. *101*, 5059–5070. https://doi.org/10.1007/s00253-017-8211-y.

64. Zong, Q.-J., Xu, T., Liu, H., Xu, L., Zhang, R.-K., Li, B.-Z., Liu, Z.-H., and Yuan, Y.-J. (2022). Microbial Valorization of Lignin to Bioplastic by Genome-Reduced *Pseudomonas putida*. Front. Microbiol. *13*, 923664. https://doi.org/10.3389/fmicb.2022.923664.

65. Salvachúa, D., Rydzak, T., Auwae, R., De Capite, A., Black, B.A., Bouvier, J.T., Cleveland, N.S., Elmore, J.R., Huenemann, J.D., Katahira, R., et al. (2020). Metabolic engineering of *Pseudomonas putida* for increased polyhydroxyalkanoate production from lignin. Microb. Biotechnol. *13*, 290–298. https://doi.org/10.1111/1751-7915.13481.

66. Lin, L., Cheng, Y., Pu, Y., Sun, S., Li, X., Jin, M., Pierson, E.A., Gross, D.C., Dale, B.E., Dai, S.Y., et al. (2016). Systems biology-guided biodesign of consolidated lignin conversion. Green Chem. *18*, 5536–5547. https://doi.org/10.1039/C6GC01131D.

67. Wang, X., Lin, L., Dong, J., Ling, J., Wang, W., Wang, H., Zhang, Z., and Yu, X. (2018). Simultaneous Improvements of *Pseudomonas* Cell Growth and Polyhydroxyalkanoate Production from a Lignin Derivative for Lignin-Consolidated Bioprocessing. Appl. Environ. Microbiol. *84*, e014699-e1518,/aem/84/18/e01469-18.atom. https://doi.org/10.1128/AEM.01469-18.

68. Green, M.R., Hughes, H., Sambrook, J., and MacCallum, P. (2012). Molecular cloning: a laboratory manual. In Molecular Cloning: A Laboratory Manual, p. 1890.

69. Boyer, H.W., and Roulland-dussoix, D. (1969). A complementation analysis of the restriction and modification of DNA in *Escherichia coli*. J. Mol. Biol. *41*, 459–472. https://doi.org/10.1016/0022-2836(69)90288-5.

70. Schäfer, A., Tauch, A., Jäger, W., Kalinowski, J., Thierbach, G., and Pühler, A. (1994). Small mobilizable multi-purpose cloning vectors derived from the *Escherichia coli* plasmids pK18 and pK19: selection of defined deletions in the chromosome of *Corynebacterium glutamicum*. Gene *145*, 69–73. https://doi.org/10.1016/0378-1119(94)90324-7.

71. Herrero, M., De Lorenzo, V., and Timmis, K.N. (1990). Transposon vectors containing non-antibiotic resistance selection markers for cloning and stable chromosomal insertion of foreign genes in gram-negative bacteria. J. Bacteriol. *172*, 6557–6567. https://doi.org/10.1128/jb.172.11.6557-6567.1990.

72. Zobel, S., Benedetti, I., Eisenbach, L., De Lorenzo, V., Wierckx, N., and Blank, L.M. (2015). Tn7-Based Device for Calibrated Heterologous Gene Expression in *Pseudomonas putida*. ACS Synth. Biol. *4*, 1341–1351. https://doi.org/10.1021/acssynbio.5b00058.

73. Martínez-García, E., and de Lorenzo, V. (2011). Engineering multiple genomic deletions in Gram-negative bacteria: Analysis of the multi-resistant antibiotic profile of *Pseudomonas putida* KT2440. Environ. Microbiol. *13*, 2702–2716. https://doi.org/10.1111/j.1462-2920.2011.02538.x.

74. Bagdasarian, M., Lurz, R., Rückert, B., Franklin, F.C., Bagdasarian, M.M., Frey, J., and Timmis, K.N. (1981). Specific-purpose plasmid cloning vectors. II. Broad host range, high copy number, RSF1010-derived vectors, and a host-vector system for gene cloning in *Pseudomonas*. Gene *16*, 237–247. https://doi.org/10.1016/0378-1119(81)90080-9.

75. Choi, K.-H., Kumar, A., and Schweizer, H.P. (2006). A 10-min method for preparation of highly electrocompetent *Pseudomonas aeruginosa* cells: Application for DNA fragment transfer between chromosomes and plasmid transformation. J. Microbiol. Methods *64*, 391–397. https://doi.org/10.1016/j.mimet.2005.06.001.

76. Weber, E., Engler, C., Gruetzner, R., Werner, S., and Marillonnet, S. (2011). A modular cloning system for standardized assembly of multigene constructs. PLoS One *6*, e16765. https://doi.org/10.1371/journal.pone.0016765.

77. Bird, J.E., Marles-Wright, J., and Giachino, A. (2022). A User's Guide to Golden Gate Cloning Methods and Standards. ACS Synth. Biol. *11*, 3551–3563. https://doi.org/10.1021/acssynbio.2c00355.

78. Blázquez, B., León, D.S., Torres-Bacete, J., Gómez-Luengo, Á., Kniewel, R., Martínez, I., Sordon, S., Wilczak, A., Salgado, S., Huszcza, E., et al. (2023). Golden Standard: a complete standard, portable, and interoperative MoClo tool for model and non-model proteobacteria. Nucleic Acids Res. *51*, e98. https://doi.org/10.1093/nar/gkad758.

79. Manoli, M.-T., Blanco, F.G., Rivero-Buceta, V., Kniewel, R., Alarcon, S.H., Salgado, S., and Prieto, M.A. (2023). Heterologous constitutive production of short-chain-length polyhydroxyalkanoates in *Pseudomonas putida* KT2440: the involvement of IbpA inclusion body protein. Front. Bioeng. Biotechnol. *11*, 1275036. https://doi.org/10.3389/fbioe.2023.1275036.

80. Tiso, T., Sabelhaus, P., Behrens, B., Wittgens, A., Rosenau, F., Hayen, H., and Blank, L.M. (2016). Creating metabolic demand as an engineering strategy in *Pseudomonas putida* – Rhamnolipid synthesis as an example. Metab. Eng. Commun. *3*, 234–244. https://doi.org/10.1016/j.meteno.2016.08.002.

81. Escapa, I.F., García, J.L., Bühler, B., Blank, L.M., and Prieto, M.A. (2012). The polyhydroxyalkanoate metabolism controls carbon and energy spillage in *Pseudomonas putida*. Environ. Microbiol. *14*, 1049–1063. https://doi.org/10.1080/10439463.2015.1016942.

82. Schneider, C.A., Rasband, W.S., and Eliceiri, K.W. (2012). NIH Image to ImageJ: 25 years of image analysis. Nat. Methods *9*, 671–675. https://doi.org/10.1038/nmeth.2089.

83. Heirendt, L., Arreckx, S., Pfau, T., Mendoza, S.N., Richelle, A., Heinken, A., Haraldsdóttir, H.S., Wachowiak, J., Keating, S.M., Vlasov, V., et al. (2019). Creation and analysis of biochemical constraint-based models using the COBRA Toolbox v.3.0. Nat. Protoc. *14*, 639–702. https://doi.org/10.1038/s41596-018-0098-2.

84. Ebrahim, A., Lerman, J.A., Palsson, B.O., and Hyduke, D.R. (2013). COBRApy: COnstraints-Based Reconstruction and Analysis for Python. BMC Syst. Biol. *7*, 74. https://doi.org/10.1186/1752-0509-7-74.

85. Burgard, A.P., Pharkya, P., and Maranas, C.D. (2003). Optknock: A bilevel programming framework for identifying gene knockout strategies for microbial strain optimization. Biotechnol. Bioeng. *84*, 647–657. https://doi.org/10.1002/bit.10803.

86. Kenefake, D., Armingol, E., Lewis, N.E., and Pistikopoulos, E.N. (2022). An improved algorithm for flux variability analysis. BMC Bioinf. *23*, 550. https://doi.org/10.1186/s12859-022-05089-9.

87. Feist, A.M., Zielinski, D.C., Orth, J.D., Schellenberger, J., Herrgard, M.J., and Palsson, B.Ø. (2010). Model-driven evaluation of the production potential for growth-coupled products of *Escherichia coli*. Metab. Eng. *12*, 173–186. https://doi.org/10.1016/j.ymben.2009.10.003.

STAR★METHODS

KEY RESOURCES TABLE

REAGENT or RESOURCE	SOURCE	IDENTIFIER
Bacterial and virus strains		
For strains constructed in this work please refer to Table S1	This work	N/A
Chemicals, peptides, and recombinant proteins		
Ampicillin	Roche	Catalog number: 10835269001-50G
Kanamycin sulfate	Roche	Catalog number: 10106801001-5G
Chloramphenicol	Sigma-Aldrich	Catalog number: C-0378-5G
Streptomycin sulfate	Sigma-Aldrich	Catalog number: S-9137-25G
IPTG (Isopropyl-b-D-thiogalactopyranosie)	Roche	Catalog number: 11411446001
X-GAL (5-Bromo-4-chloro-3-indolyl β-D-galactopyranoside)	Roche	Catalog number: 10703729001
m-Toluic acid (3-methyl benzoic acid)	Sigma-Aldrich	Catalog number: 89890
BpiI (BbsI) (10U/μL)	Thermo Fisher Scientific	Catalog number: ER1012
BsaI (Eco31I) (10U/μL)	Thermo Fisher Scientific	Catalog number: ER0291
T4 DNA ligase	New England Biolabs (NEB)	Catalog number: M0202L
Sodium 4-hydroxybenzoate	Sigma-Aldrich	Catalog number: H-3766-25G
Sodium octanoate	Sigma-Aldrich	Catalog number: C5038-500G
Sulfuric Acid	Sigma-Aldrich	Catalog number: 1120801000
Critical commercial assays		
MoClo Toolkit	(Weber et al.)[76]	Addgene: Kit # 1000000044 https://www.addgene.org/kits/marillonnet-moclo/
QUIAquick Gel Extraction Kit (250)	Quiagen	Catalog number: 28706
High pure RNA isolation kit (50)	Roche	Catalog number: 11828665001
DNA-free kit DNase Treatment and Removal Reagents	Ambion	Catalog number: AM1906
Transcriptor 1st strand cDNA kit (200)	Roche	Catalog number: 04897030001
Lightcycler 480 SYBR GREEN I Master (10 × 5 mL)	Roche	Catalog number: 04887352001
Deposited data		
Metabolic models	N/A	Github Repository (models folder) https://github.com/SBGlab/PET2PHA/tree/main/models
Computational workflow results	N/A	Github Repository (data folder) https://github.com/SBGlab/PET2PHA/tree/main/data
Code	N/A	Github Repository (code folder) https://github.com/SBGlab/PET2PHA/tree/main/code
Experimental models: Organisms/strains		
Pseudomonas putida KT2440; TOL plasmid-curated, spontaneous restriction deficient derivative of *P. putida* mt-2	Bagdasarian et al.[74]	ATCC 47054/DSM 6125
Escherichia coli DH10B; Cloning host; F-, mcrA Δ(mrr hsdRMS-mcrBC) Φ80dlacΔM15 ΔlacX74 deoR recA1 araD139 Δ(ara-leu)7697	Invitrogen, Thermo Fisher Scientific, USA	N/A

(*Continued on next page*)

Continued

REAGENT or RESOURCE	SOURCE	IDENTIFIER
Escherichia coli CC118λ*pir; Rfr,Spr Cloning host; Δ(ara-leu), araD, ΔlacX74, galE, galK, phoA20, thi-1, rpsE, rpoB, argE (Am), recA1, lysogenized with λpir phage*	(Herrero et al.)[71]	N/A
Escherichia coli HB101; Helper strain; F- λ- hsdS20(rB- mB-) recA13 leuB6(Am) araC14 Δ(gpt-proA)62 lacY1 galK2(Oc) xyl-5 mtl-1 rpsL20(SmR) glnX44(AS)	(Boyer et al.)[69]	DSM 1607
Escherichia coli DH5a; F- phi80d lacZDeltaM15 endA1 recA1 hsdR17 (rk-mk-) supE44 thi-l lambda- gyrA96 relA1 Delta(lacZYA-argF)U169. Host for pUC or other alpha complementing vectors, pBR322; for cDNA cloning	Zobel et al.[72]	DSM 6897
Oligonucleotides		
For oligonucleotides sequence please refer to Table S8	This work	N/A
Recombinant DNA		
For plasmids used in this work please refer to Table S1	This work	N/A
Software and algorithms		
ImageJ	Schneider et al.[82]	https://imagej.nih.gov/ij/
ChemDraw 21.0	PerkinElmer	https://revvitysignals.com/products/research/chemdraw
Corel Draw X7	N/A	https://www.coreldraw.com/la/?link=wm
Inkscape	N/A	https://inkscape.org/es/
Biorender	N/A	https://www.biorender.com/
MATLABR2010b	Mathworks	https://es.mathworks.com/products/matlab.html
GraphPad Prism 6.0	GraphPad Software	https://www.graphpad.com/scientific-software/prism/
Zotero	N/A	https://www.zotero.org/
Benchling	N/A	https://www.benchling.com/
Escher for metabolic fluxes distribution visualization	Escher	https://escher.github.io
gcFront	Legon et al.[39]	https://github.com/lLegon/gcFront
cameo	N/A	https://github.com/biosustain/cameo
cobrapy	N/A	https://github.com/opencobra/cobrapy
straindesign	N/A	https://github.com/klamt-lab/straindesign
Jupyter Notebook	N/A	https://github.com/jupyter/notebook
In-house software	N/A	https://github.com/SBGlab/PET2PHA
Models used in this work	This work	https://figshare.com/articles/software/PET2PHA_Source_code_and_resources_for_in_silico_metabolic_analysis_in_P_putida_to_accumulate_PHA_with_PET_as_carbon_source/23760606/1

RESOURCE AVAILABILITY

Lead contact

Further information and requests for resources and reagents should be directed to and will be fulfilled by the Lead Contact Dr. Juan Nogales (jnogales@cnb.csic.es).

Materials availability

Plasmids generated in this study are available from the lead contact with a completed Materials Transfer Agreement. This study did not generate unique reagents. Please refer to key resources table for the reagents and data generated in this work.

Data and code availability

- All the data that support the findings of this study is available in the data folder within the PET2PHA repository at https://doi.org/10.6084/m9.figshare.23760606.v1. These data were derived from the resources mentioned in the *Deposited data* and *Software and algorithms* section in the key resources table and from the in-house software developed.
- All the original code has been deposited through a figshare repository, including in-house software specifically developed for this study. Everything is available in the code folder within the PET2PHA repository at https://doi.org/10.6084/m9.figshare.23760606.v1.
- Any additional information required to reanalyze the data reported in this work paper is available from the lead contact upon request.

EXPERIMENTAL MODEL AND STUDY PARTICIPANT DETAILS

The experimental model used in this work are bacterial strains of *E. coli* and *P. putida*, please refer to key resources table section: *Experimental models: Organisms/strains*.

Bacterial strains, media and culture conditions

Bacterial strains and plasmids used in this work are listed in Table S1. *E. coli* and *P. putida* strains were grown routinely for DNA manipulations and pre-cultures in lysogeny broth (LB) medium at 37°C and 30°C, respectively.[68] The appropriate selection of antibiotics, ampicillin (Amp, 100 μg/mL), chloramphenicol (34 μg/mL), kanamycin (Km, 50 μg/mL), streptomycin (75 μg/mL), IPTG (0.5–1 mM) and Xgal (40 μg/mL) were added where needed.

Standard growth experiments of *P. putida* in the defined medium were performed in M63 minimal medium (13.6 g/L KH_2PO_4, 2 g/L $(NH_4)_2SO_4$, 0.5 mg/L $FeSO_4 \times 7\ H_2O$, adjusted to pH 7.0 with KOH), supplemented with the carbon source needed in each case for 24 h at 30°C under vigorous shaking at 200 rpm.[17] The medium was supplemented with 1 mM $MgSO_4$ and 1X solution of trace elements (Goodies) (composition 1000X dissolved in 1N HCl: 2.78 g/L $FeSO_4 \times 7H_2O$, 1.98 g/L $MnCl_2 \times 4H_2O$, 2.81 g/L $CoSO_4 \times 7H_2O$, 1.47 g/L $CaCl_2 \times 2H_2O$, 0.17 g/L $CuCl_2 \times 2H_2O$, 0.29 g/L $ZnSO_4 \times 7H_2O$).

For TPA and EG co-feeding experiments, we followed the Tiso and collaborators assay with some modifications.[57] For this, the Delft minimal medium was used (3.88 g/L K_2HPO_4, 1.63 g/L NaH_2PO_4, 2 g/L $(NH_4)_2SO_4$, adjusted to pH 7.0 with KOH) supplemented with a synthetic mixture of 20 mM TPA and 20 mM EG. The medium was supplemented with 1X solution of Delft trace elements dissolved in 1N HCl and pH adjusted to 4 and filtered (composition of 100X: 0.5 g/L $FeSO_4 \times 7H_2O$, 0.1 g/L $MnCl_2 \times 2H_2O$, 0.04 g/L $CoCl_2 \times 6H_2O$, 0.1 g/L $CaCl_2 \times 2H_2O$, 0.02 g/L $CuSO_4 \times 5H_2O$, 0.2 g/L $ZnSO_4 \times 7H_2O$, 10 g/L $MgSO_4 \times 6H_2O$, 1 g/L EDTA, 0.02 g/L $Na_2MoO_4 \times 2H_2O$).

For PET hydrolysate assays, concentrated 1000X PET hydrolysate from Tiso and collaborators[57] was used and supplemented with 2 g/L $(NH_4)_2SO_4$ and 1X solution of Delft trace elements. This synthetic mix was properly diluted to 1X with water by adjusting the pH to 7.3 with 1N NaOH and filtered. To avoid TPA precipitations, this synthetic mix was properly prepared the date of experiment and resulted to final concentration of 17–22 mM EG and 18–33 mM TPA.

METHOD DETAILS

Physiological studies and parameters calculation

For *P. putida* growth experiments, LB pre-culture cells were washed twice with 0.85% saline solution and adjusted to an optical density of 600 nm of 0.3 M63 minimal medium supplemented with 5 mM sodium 4-hydroxybenzoate (C/N = 1.12 mol/mol) and with the presence of 3 mM octanoate (C/N = 2 mol/mol). Culture growth (50 mL) was monitored in Erlenmeyer shaking flasks (200 rpm) of 250 mL using a portable spectrophotometer (Fischer Scientific, Pennsylvania, USA) at 600 nm for 24 or 48 h.

In all the experimental approaches, the cultures occupied no more than 20% of the volume of the flask and special care was taken to control the C/N ratio in order to compare the different growth conditions when several carbon sources were applied. For balanced conditions (without nitrogen limitation), the C/N ratio was between 1 and 3 mol/mol, whereas for the traditional PHA accumulation experiments (including nitrogen limitation), the C/N ratio was maintained at 40 mol/mol.

Construction of *P. putida* engineered strains

Standard molecular biology techniques were performed.[68,69] The genes of interest were inactivated by allelic exchange homologous recombination using the mobilizable plasmid pK18*mobsacB*.[20,70] Briefly, PCR primer pairs (Table S8) were designed to amplify approximately 800 bps regions upstream (Z1) and downstream (Z3) of the deleted gene to serve as homology recombination arms. Appropriate restriction enzyme sites were added upstream of Z1 and downstream of Z3 to clone the fragment Z1Z3 into pK18*mobsacB*. The resulting pK18*mobsacB*-Z1Z3 construction was introduced into *P. putida* KT2440's genome by using the

triparental filter-mating technique.[71] For the first recombination selection process, cetrimide agar plates supplemented with 50 μg/mL kanamycin were used, allowing only the selection of *Pseudomonas* strains.[72] The resulting recombinant strains were confirmed by PCR and selected colonies were grown in LB for 6 h and then plated on M63 minimal medium plus 20 mM glucose selective plates supplemented with 5% sucrose. Transconjugants sucrose-resistant and kanamycin-sensitive were isolated and the second recombination event was confirmed by PCR using external primers of the arms of homology region, and DNA sequencing (Table S8).

For the *pha* cluster deletion, the pEMG knockout system was used, with some modifications.[73,74] *P. putida* transconjugants of the first recombination event were transformed with pSW-I via electroporation. The selection plates were LB + 500 μg/mL Amp and 15 mM 3-methylbenzoate (3MB), and incubated at 30°C for 16 h. We should note here, that KT2440 is naturally resistant to ampicillin but such concentration allows plasmid selection. Additionally, the I-Sce-I endonuclease expression is dependent on a 3MB inducible promoter system. Single colonies were picked on LB + 500 μg/mL Amp and LB + Km to screen for kanamycin-sensitive clones. Similar to pK18*mobsaB* strategy, several kanamycin-sensitive clones were checked for the knockout phenotypes, using external primers to the homology region (FdPHA and RdPHA, Table S8). To confirm, the integrity of the homology region, DNA sequencing of the PCR product was performed. Under non-selective cultivation *Pseudomonas* lose the pSW-I plasmid quite fast. For this purpose, several single colonies were checked for 500 μg/mL Amp sensitivity to verify pSW-I plasmid loss.

For TPA growth cultures the pRK190 plasmid was generated. This derives from the pBT'T_*tph* plasmid harboring the *tph* operon codifying the *pcaRtphA2A3B1A1pcaK* genes for TPA degradation from *Pseudomonas umsongensis* GO16.[50] Briefly, the synthetic *tph* operon and expression vector (pBT'T, kanamycin resistance, constitutive expression, low copy number) were amplified by PCR and joined via Gibson assembly. The full assembly reaction was transformed in *E. coli* DH5α. Plasmid constructs, extracted from positive transformant colonies, were used for subcloning of the *pha* synthetic operon derived from pMM55 via NotI, generating pRK190 plasmid. The confirmed plasmid constructs were electroporated in electrocompetent *P. putida* engineered strains prepared as described previously.[75]

Golden gate/MoClo plasmid construction

Golden gate cloning method is based on the use of type IIS restriction enzymes combined with restriction-ligation, which allows high cloning efficiency using a single one-pot step.[76–78] Golden gate/MoClo plasmids (Table S1) were constructed following the Weber et al. protocol with some modifications.[76,78,79] Briefly, for Level 0 plasmid construction, every part was PCR amplified with oligonucleotides designed with the Benchling platform (www.benchling.com) with the following characteristics: a tail containing the BpiI recognition site followed by the corresponding 4-nt fusion site, 21 bp of minimal length for target complementarity, 50°C of minimal Tm for that region and a maximal Tm difference of ±1.5°C between both oligonucleotides. If a part contained a BpiI/BsaI recognition site, it would be eliminated introducing by PCR amplification silent same sense point mutations in the restriction site sequences.

The position and orientation of each gene in a final construct determines which level 1 destination vector has to be chosen for the assembly of a transcription unit. These level 1 vectors differ only by the sequence of the fusion sites. The two external fusion sites (BpiI cleavage sites) of each vector are designed to be compatible with the fusion sites of the vectors from the position before and after.

Level 2 vectors contain two inverted BpiI recognition sites for insertion of level 1 modules. The upstream fusion site (TGCC) is compatible to a gene cloned in a level 1 vector, whereas the downstream fusion site consists of a universal sequence (GGGA). This design allows the cloning of two to six genes in the same vector. The last gene is fused to the vector by using a compatible linker. During each step of the part construction, apart from the control digestion process, sequencing of all the included parts was realized.

The correct level 2 plasmids with compatible origin of replication were transformed into *P. putida* strains following the Choi et al. protocol with some adaptations.[75] Briefly, *P. putida* strains were grown overnight in 10 mL of LB at 30°C and vigorous shaking at 200 rpm. These cultures were pelleted at 3,200 ×*g* for 10 min, washed five times with 300 mM sucrose and resuspended in 300 μL of 300 mM sucrose. 100 μL of cell suspension were mixed with 100 ng of the desired plasmid and transferred to a 2 mm gap electroporation cuvette. After a pulse of 25 μF, 2.5 kV and 200 Ω; 900 μL of room temperature LB was added and transferred to a 100 × 16 mm round-bottom polypropylene tube, and incubated for 1 h at 30°C, 200 rpm. 100 μL of the 1/10 diluted transformation cultures were plated on LB agar plates containing the corresponding antibiotic for the plasmid maintenance, and grown at 30°C.

For the purpose of this work, the SynPro16 promoter was used with an upstream λT0 terminator which was introduced into the Golden gate-MoClo pL0-PU plasmid.[79,80] Genes encoding PhaC1, PhaF, PhaG, and AlkK enzymes from *P. putida* KT2440 were cloned into the pL0-SC plasmid from the Golden gate-MoClo kit. The terminators λT1, rnpB-T1, and rpoC-term were cloned into the pL0-T plasmid from the Golden gate-MoClo kit.

RNA extraction and real-time qPCR experiments

For the RNA extraction process, standard molecular biology techniques were followed.[20,81] The RNA samples were obtained after 6 h of growth (at mid-exponential phase), and 7 mL were harvested by centrifugation at 3000 x*g* for 10 min at 4°C. The cell pellets were rapidly frozen in dry ice and stored at −80°C until further use. Pellets were resuspended in TE buffer (10 mM Tris-HCl pH 7.5, 1 mM EDTA) containing 5 mg/mL of lysozyme. RNA was extracted using the High Pure RNA Isolation kit (Roche) following the manufacturer's instructions. Extracted RNA was additionally treated with DNase (Ambion) following the manufactureŕs instructions. RNA integrity was checked by agarose gel electrophoresis and was quantified with NanoDrop 2000 Spectrophotometer (Thermo Scientific, Massachusetts, USA).

cDNA synthesis was performed using the Transcriptor First Strand cDNA Synthesis kit (Roche), following the manufacturés recommendations. cDNA was synthesized from 1 μg of purified RNA using random hexamer-primed reactions. For the real-time qPCR reaction, 1 μg of transcribed cDNA was used and a standard curve of differential dilutions (from 10^{-1} to 10^{-5}) of *P. putida* genomic DNA was plotted. The sequence of the primers used for this study is listed in Table S8. For the data analysis, the absolute quantification was chosen, showing the expression levels in nM concentration of cDNA. This analysis was performed in three technical replicates from two independent biological samples and the size of each amplified gene was considered.

PHA determination by methanolysis and GC-MS analysis

For composition and total cellular PHA content quantification, standard GC-MS approaches of the methanolized polyester were used.[20,79] In each condition, at least two independent biological replicates were performed. Where the statistical error was higher of 10%, three biological replicates were performed. During the methanolysis process, two technical replicates were included for each biological sample. Briefly, 2–5 mg of lyophilized samples (culture pellets) were resuspended in 2 mL of methanol containing 15% sulfuric acid and 2 mL of chloroform containing 0.5 mg/mL 3-methylbenzoic acid (3MB) as internal standard and then incubated using a screw-capped tube at 100°C for 5 h. After cooling, a two-phase extraction process was performed, followed by the addition of a small amount of Na_2SO_4 powder to completely remove the water phase. The organic phase containing the resulting methyl esters of monomers was analyzed by GC-MS.

An Agilent (Waldbronn, Germany) series 7890A gas chromatograph coupled with a 5975C MS detector (EI, 70 eV) and a split–splitless injector were used for the analyses.[20] During this work, the DB-5HTDB-5HT column (400°C: 30 m × 0.25 mm x 0.1 μm film thickness) was used. The retention time for each methyl ester monomer obtained in this work was 3.5 min (C6), 7.2 min (C8) (C7:1), 7.2 min (C8), 9.3 min (C9:1), 12.0 min (C10), 14.1 min (C11:1), 16.2 min (C12:1), 16.6 min (C12), 20.9 min (C14) and 6.1 min (3MB, internal standard).

TPA quantification using HPLC-MS

TPA samples were collected after culture centrifugation at 15,000 x*g* for 10 min. Then, supernatants were diluted 10 times before being injected in the HPLC Agilent 1260 series apparatus (Agilent, USA) equipped with SQ mass spectrometer. The related metabolites were separated on a C18 LC column (Agilent Poroshell 120 EC-C18 column (34.6 mm × 100 mm; particle size 4 μm) at 30°C and a flow rate of 1 mL/min. The following gradients of buffer A (water acidified with 0.1% formic acid) and buffer B (20% acetonitrile acidified with 0.1% formic acid) were used: starting with a mobile phase of 100 of A, the B concentration was ramped linearly to 40% in 12 min, then returned back to 100% of A and maintained constant at 100% for 2 min. The TPA was detected at 230 nm with the quantifications being realized using external standards and by mass spectroscopy. The standard curves were generated by measuring 1–100 mM TPA.

Extracellular metabolites identification by HPLC

The presence of residual 4-hydroxy benzoate (4HBz; Sigma-Aldrich, Merck, Germany) was quantified by HPLC (Agilent Series 1260 Infinity II, Agilent, CA, USA), on a ZORBAX Eclipse Plus C18 (Biorad, Hercules, CA, USA, Agilent, CA, USA) at room temperature with a flow rate of 0.5 mL min^{-1} and an injection volume of 25 μL. The mobile phase was 0.1% trifluoroacetic acid in water (A) and 0.1% trifluoroacetic acid in methanol (B). The following elution program was used as follows: at the start, 85% A and 15% B; after 11 min, the percentage of B was linearly increased to 50%. After that, it was ramped to the original composition in 2 min and then equilibrated for 8 min. The retention time of 4HBz was 13.5 min. A standard curve of 4HBz was done (1–5 mM). As a control, the medium without 4HBz was injected.

For EG quantification, the same liquid chromatography technique was used, but in this case with an ion exchange column Aminex HPX-87H (Bio-Rad, Hercules, CA, USA) at 50°C with a 0.6 mL/min flow rate and a 25-μL injection volume. The mobile phase was 5 mM of sulfuric acid applied on an isocratic regimen, and compounds were detected by means of a refractive index detector. For the standard curve 1–100 mM EG was used. The retention time of EG was of 14.5 min.

Microscopy assays

Cultures were routinely visualized with a 100X phase-contrast objective (Nikon microscope) and images were taken with an attached camera (Leica DFC345 FX).

For transmission electron microscopy (TEM) assays, *P. putida* cells previously grown under PHA production conditions for 24 h were harvested and washed twice in 1X PBS as previously described.[79] Briefly, the cells were fixed for 1 h in 3% glutaraldehyde in PBS and then washed twice with PBS. Samples were post-fixed in 1% osmium tetroxide and 0.8% potassium ferricyanide for 1 h at 4°C. Samples were washed with PBS prior to dehydration with an increasing gradient of ethanol (30%, 50%, 70%, 80%, 90% and 100%) of 10 min per step. Samples were embedded in LX112 resin and were polymerized for 48 h at 60°C. 60–80 nm sections were placed in copper grids of 75 mesh and stained with 5% uranyl acetate for 15 min and lead citrate for 3 min. Samples were viewed in a JEOL 1230 TEM and images were taken with a CMOS TVIPS 16 mp camera. For pictures schematic representation ImageJ software was used for analysis.[82]

Constraint-based flux analysis

P. putida models[26,51] were analyzed with the COBRA Toolbox v3.0 within the MATLAB environment (The MathWorks Inc.)[83] and COBRApy package (version 0.25.0).[84] Tomlab CPLEX and the GNU Linear Programming kit were used for solving linear programming problems. The constraint-based model consists of an m x n matrix containing all the stoichiometric coefficients in the models of m metabolites and n reactions (S).

Flux balance analysis (FBA) is a widely used approach for studying biochemical networks, in particular GEMs. FBA calculates the flow of metabolites through the given metabolic network, making it possible to analyze the phenotypes and capabilities of organisms with different environmental or genetic perturbations, to predict the growth rate of an organism or the rate of production of a metabolite of interest.

Model-driven design of growth-coupled PHA strains

We addressed the identification of growth-coupled *in silico* overproducing PHA designs using PET as the sole carbon source by using gcFront,[39] presenting several advantages over previous methods. First, it is an algorithm that explores knockout (KO) strategies that simultaneously maximize cell growth, product synthesis, and coupling strength (tri-level optimization). The incorporation of this last optimization parameter significantly reduces the search time compared to other widely used strain designing algorithms such as OptKnock[85] thus, speeding up the discovery of KO strategies.[39] In addition, gcFront selects strategies by using a genetic algorithm, therefore it is able to generate many alternative optimal and suboptimal designs on the pareto surface during a single run, efficiently exploring the available metabolic design space, and leaving the user flexibility in selecting t87he designs to be applied in the laboratory.

In order to reduce the computational complexity of the analysis, before applying gcFront, we proceeded to construct a simplified version of *i*JNP4SB, following the workflow shown in Figure 2. The reduced model was constructed by applying two consecutive simplification steps e.g., model simplification and model reduction. This simplified model version included a less complex biomass equation and a reduced PHA and alginate metabolism, e.g., only the final production of mcl-PHA containing 8 carbon atoms (C8), and a specific single alginate (alginate with 3 units of acetylated D-mannuronate and 2 units of L-guluronate) were considered. Lumped reactions corresponding to pyruvate dehydrogenase, 2-oxoglutarate dehydrogenase, and TOL plasmid reactions were also removed from the simplified model. To avoid unrealistic acetate secretion, the boundaries of the reactions ALDD2x (aldehyde dehydrogenase acetaldehyde), CYSS (cysteine synthase), and NACODA (N-acetylornithine deacetylase), which produce acetic acid from acetaldehyde, O-acetyl-L-serine and N-acetyl-L-glutamate 5-semialdehyde, respectively, were set up to 0. Additionally, the boundaries of the reactions PHADPC80 (poly-3-hydroxyalkanoate depolymerase C80) and RHACOAE80 (*R*-hydroxyacyl-CoA thioesterase C80) involved in the production of *R*-hydroxy acids were also set up to 0.

In the following step, the blocked reactions when using PET as a carbon source were identified by means of Flux Variability Analysis (FVA) using up to 20% of the maximal growth rate and removed from the simplified model.[86] For clarification, the blocked reaction in a metabolic network refers to a reaction that does not participate in any optimization solution and can be defined with a minimum and maximum theoretical flux lower than 10^{-6} mmol·gDW^{-1}·h^{-1}. Finally, the list of target reactions to be deleted (KO reaction list) was constructed by applying four additional and iterative reduction steps including the removal of: (i) reactions encoded by essential and/or nearly-essential genes, (ii) all reactions without associated genes in the model, (iii) peripheral and transport reactions, and (iv) the sets of flux-coupled reactions were aggregated as a single reaction (Figure 2).[87] To further increase the searching speed of gcFront, we run the strain designing algorithm OptKnock using the KO reaction list allowing a maximum number of deletions between 3 and 5. From the more promising OptKnock strategies, key reactions were collected to construct a more reduced target reactions list (reduced KO reaction list).

The generation of the reduced KO reaction list involved the execution of OptKnock with varying KO and carbon limits (C). Iteratively following the steps outlined within the yellow box (Figure 2), each parameter combination resulted in a distinct candidate list. The KO limit controlled the maximum number of deletions applied to the model, while the C limit excluded reactions within peripheral pathways from the KO reaction list due to their minimal impact on growth-coupled (GC) strategies. Subsequently, strategies were evaluated based on the flux of the target reaction and model growth. Strategies yielding less than 10% of initial growth and/or less than 0.05 mmol/DW/h of flux in the target reaction were filtered out. From the remaining strategies, a reaction ranking was generated, ultimately resulting in the creation of the final candidate list referred to as the reduced KO reaction list. Finally, gcFront set the maximum number of knockouts to 30. The rest of parameters used to configurate gcFront are shown in Table S2.

In silico manual curation for candidate's selection

The performance of growth-coupled strain designs obtained through our in-house pipeline for the bioproduction task proposed in this study is depicted within the production envelope of the wild-type (WT) strain (Figure 3). The designs are color-coded based on our proposed design score, which equally considers coupling strength (as defined in the gcFront) and biomass-coupled product yield (BCPY). From this analysis, the PET4 design stands out as the most promising candidate for further *in silico* evaluation (please also refer to the corresponding results section).

For the assessment of PET4 performance dynamic Flux Balance Analysis (FBA) analysis was performed. PET4 demonstrates the capability to produce a significant amount of PHA from PET within a reasonable time frame (50 h).

Upon selecting PET4 as our target design, we conducted a clustered impact ranking of individual reactions within PET4 to evaluate its performance. Reactions with more negative impacts (ORNCD, ICL, ICDHyr, and MALS) are essential for coupling the production of PHA to growth (minimal design). Another group of KO reactions, including FORGLUH2, MCITL2, PPCSCT, and SUCOAS, has a moderate Impact Score but lacks decoupling capability, forming together the previous reactions the intermediate design. The remaining KO reactions in the PET4 design have a negligible impact on PHA (see Table S4 for reaction nomenclature).

To evaluate the designs derived from PET4, the production envelopes of the WT strain and three different designs derived from PET4/complete are shown. It is noteworthy that the minimal design is not growth-coupled, indicating the necessity of those additional reactions included in the intermediate impact score cluster to couple PHA production with growth. As expected, the inclusion of the last group of KO reactions only slightly improves the PHA production performance.

For the generation of the metabolic map for the visualization of the distribution of metabolic fluxes, the web application Escher (https://escher.github.io) was used (Figure S1). The resulting map was saved in json format. Models used in this work are accessible through the figshare repository of the project (https://doi.org/10.6084/m9.figshare.23760606.v1).

QUANTIFICATION AND STATISTICAL ANALYSIS

In each condition, at least two independent biological replicates were performed. Where the statistical error was higher of 10%, three biological replicates were performed. During the methanolysis process, two technical replicates were included for each biological sample. The mean values and the standard deviation of these replicates is represented in the Figures and Tables of the manuscript.

Cell Reports, Volume *43*

Supplemental information

A model-driven approach to upcycling recalcitrant feedstocks in *Pseudomonas putida* by decoupling PHA production from nutrient limitation

Maria-Tsampika Manoli, Álvaro Gargantilla-Becerra, Carlos del Cerro Sánchez, Virginia Rivero-Buceta, M. Auxiliadora Prieto, and Juan Nogales

Supplementary Materials and Methods

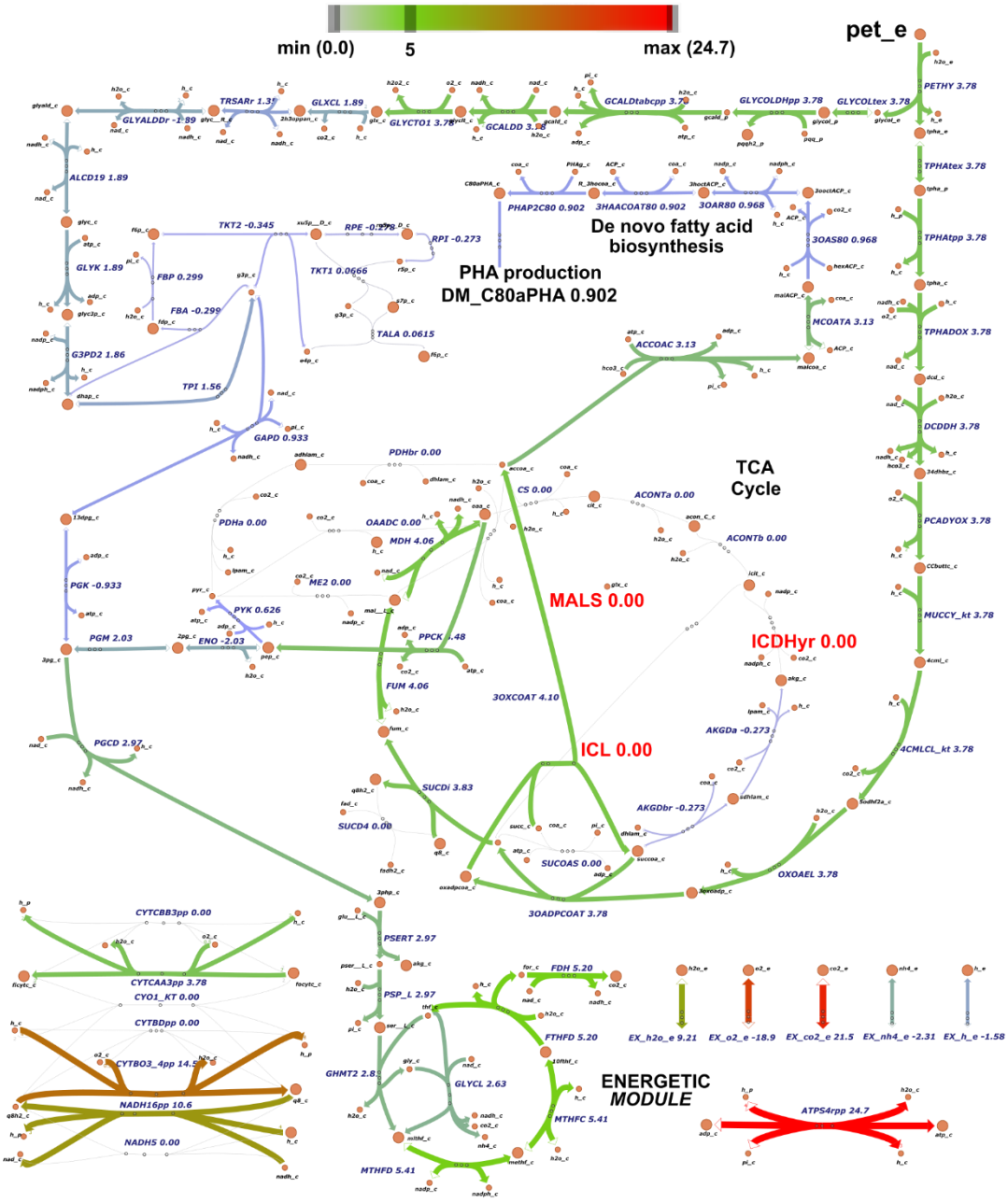


Figure S1. Predicted carbon flux distribution in PET-growth optimized intermediate design when compared with the wild-type model. The deleted reactions (in grey), the increased flux reactions (in green), the reduced flux reactions (in red), and the unaffected fluxes (blue) are shown. Related to Figure 3.

Table S1. *Pseudomonas putida* strains and plasmids used in this study. The most relevant characteristics are mentioned. Related to Star Methods bacterial strains, media and culture conditions section.

Strains	Genotype/ Relevant characteristics	Reference
KT2440	TOL plasmid-curated, spontaneous restriction deficient derivative of *P. putida* mt-2	[S1]
PP05_01	KT2440 derivative strain, Δ*pha* cluster (PP_5003-PP_5008)	CECT 30020; [S2]
PP05_18	KT2440 derivative strain, Δ*pha* cluster *gclR* (PP_5003-PP_5008 PP_4283)	This work
MM3	KT2440 derivative strain, Δ*mmgF*	This work
MM4	KT2440 derivative strain, Δ(*mmgF scpC*)	This work
MM6	KT2440 derivative strain, Δ*(mmgF scpC sucC sucD*)	This work
MM8	KT2440 derivative strain, Δ(*mmgF scpC sucC sucD aceA*)	This work
MM9	KT2440 derivative strain, Δ(*mmgF scpC sucC sucD aceA glcB*)	This work
MM11	KT2440 derivative strain, Δ(*mmgF scpC sucC sucD aceA glcB icd*)	This work
MM12	KT2440 derivative strain, Δ(*mmgF scpC sucC sucD aceA glcB icd phaZ*)	This work
MM13	KT2440 derivative strain, Δ(*mmgF scpC sucC sucD aceA glcB icd phaZ PP_3190*)	This work
MM14	KT2440 derivative strain, Δ(*mmgF scpC sucC sucD aceA glcB icd phaZ PP_3190 ocd*)	This work
MM15	KT2440 derivative strain, Δ(*mmgF scpC sucC sucD aceA glcB icd phaZ PP_3190 ocd hutF*)	This work
MM16	KT2440 derivative strain, Δ(*mmgF scpC sucC sucD aceA glcB icd phaZ PP_3190 ocd hutF PP_3533*)	This work
MM19	KT2440 derivative strain, Δ(*mmgF scpC sucC sucD aceA glcB icd phaZ PP_3190 ocd hutF PP_3533 PP_5003-PP_5008*)	This work
MM20	KT2440 derivative strain, Δ(*mmgF scpC sucC sucD aceA glcB icd phaZ PP_3190 ocd hutF PP_3533 PP_5003-PP_5008 PP_4283*)	This work
MM19 (pMM55)	Km^r, MM19 strain bearing pMM55; *pha* optimized vector	This work
PP05_01 (pMM55)	Km^r, PP05_01 strain bearing pMM55; *pha* optimized vector	This work
MM20 (pRK190)	Km^r, MM20 strain bearing pRK190; *tph-pha* optimized vector	This work
PP05_18 (pRK190)	Km^r, PP05_18 strain bearing pRK190; *tph-pha* optimized vector	This work

Plasmids	Relevant characteristics	Reference
Cloning vectors		
pRK600	Cm^r, ColE1 *oriV* RK2 Mob^+ Tra^+ donor of transfer functions	[S3]

pBT'T_*tph*	Km^r, ori pBBR1 harbouring the *pcaRtphA2A3B1A1pcaK* for TPA degradation	[S4]
pRK190	Km^r, pBT'T_*tph* derivative harbouring the *phaC1*^{Pp}, *phaF*^{Pp}, *phaG*^{Pp}, *alkK*^{Pp}	This work

pK18*mobsacB* derivative vectors

pK18*mobsacB*	Km^r, pMB1, *oriV*, Mob$^+$, *lacZa*, *sacB*; vector for allelic exchange homologous recombination mutagenesis	[S5]
pRK87	Km^r, pK18*mobsacB* derivative vector used for *mmgF* deletion	This work
pRK88	Km^r, pK18*mobsacB* derivative vector used for *scpC* deletion	This work
pRK89	Km^r, pK18*mobsacB* derivative vector used for *sucC-sucD* deletion	This work
pMM4	Km^r, pK18*mobsacB* derivative vector used for *phaZ* deletion	[S6]
pMM15	Km^r, pK18*mobsacB* derivative vector used for *aceA* deletion	This work
pMM16	Km^r, pK18*mobsacB* derivative vector used for *glcB* deletion	This work
pMM19	Km^r, pK18*mobsacB* derivative vector used for *icd* deletion	This work
pMM22	Km^r, pK18*mobsacB* derivative vector used for PP_3190 deletion	This work
pMM24	Km^r, pK18*mobsacB* derivative vector used for *hutF* deletion	This work
pMM25	Km^r, pK18*mobsacB* derivative vector used for *ocd* deletion	This work
pMM26	Km^r, pK18*mobsacB* derivative vector used for *PP_3533* deletion	This work
pMM52	Km^r, pK18*mobsacB* derivative vector used for *PP_4283* deletion	This work

pEMG deletion strategy vectors

pEMG	Km^r, plasmid used for deletions; *ori* R6K *oriV*, *lacZα* fragment with two flanking I-SceI recognition sites	[S7]
pEMGTS1-TS2	Km^r, pEMG derivative vector used for *pha* cluster deletion	[S8]
pSW-I	Amp^r, helper plasmid used for deletions; *ori* RK2, *oriV*, xylS, Pm→I-SceI	[S9]

Golden gate cloning vectors level 0

pICH41295	Sm^r, *ori* pMB1/ColE1, golden gate cloning vector level 0_ promoter region	Addgene, USA
pICH41308	Sm^r, *ori* pMB1/ColE1, golden gate cloning vector level 0_ coding sequence region	Addgene, USA
pICH41276	Sm^r, *ori* pMB1/ColE1, golden gate cloning vector level 0_ terminator region	Addgene, USA
pRK154	Sm^r, pICH41295 derivative vector, λT0-SynPro16 promoter	[S10]
pSS14	Sm^r, pICH41276 derivative vector, λT1 terminator	[S10]
pRK106	Sm^r, pICH41276 derivative vector, rnpB-T1 terminator	[S10]
pRK107	Sm^r, pICH41276 derivative vector, rpoC term terminator	[S10]
pSS68	Sm^r, pICH41308 derivative vector, *phaF* gene (PP_5007)0	This work
pSS70	Sm^r, pICH41308 derivative vector*, phaC1* gene (PP_5003)	This work
pMM32	Sm^r, pICH41308 derivative vector*, phaG* gene (PP_1408)	This work

pMM33	Sm^r, pICH41308 derivative vector, *alkK* gene (PP_0763)	This work
Golden gate cloning vectors level 1		
pICH47732	Amp^r, *ori* pUC/RK2, golden gate cloning vector level 1 position 1	Addgene, USA
pICH47742	Amp^r, *ori* pUC/RK2, golden gate cloning vector level 1 position 2	Addgene, USA
pICH47751	Amp^r, *ori* pUC/RK2, golden gate cloning vector level 1 position 3	Addgene, USA
pICH47761	Amp^r, *ori* pUC/RK2, golden gate cloning vector level 1 position 4	Addgene, USA
pICH47772	Amp^r, ori pUC/RK2, golden gate cloning vector level 1 position 5	Addgene, USA
pICH54033	Amp^r, *ori* pUC/RK2, golden gate cloning vector level 1 position 3; dummy	Addgene, USA
pMM34	Amp^r, pICH47732 derivative vector level 1 position 1; T0-SynPro16-*phaC1*-λT1	This work
pMM35	Amp^r, pICH47742 derivative vector level 1 position 2; T0-SynPro16-*phaF*-rnpB-T1	This work
pMM37	Amp^r, pICH47772 derivative vector level 1 position 5; T0-SynPro16-PP_0763-λT1	This work
pMM38	Amp^r, pICH47761 derivative vector level 1 position 4; T0-SynPro16-*phaG*-rnpB-T1	This work
Golden gate cloning vectors level 2		
pAGM4723	Km^r, *ori* ColE1/pVS1, golden gate cloning vector level 2	Addgene, USA
pICH49299	Amp^r, *ori* pUC/RK2, golden gate vector level 2 end-linker (open construct), position 5	Addgene, USA
pMM55	Km^r, pAGM4723 derivative vector level 2; *phaC1*; *phaF*; dummy 3; *phaG*; PP_0763	This work

Table S2. gcFront parameters whose default values have been changed for convenience. Abbreviations: R, model reactions set; C, candidate reactions set. Related to Figure 2.

gcFront Parameter	Value
biomassrxn	BiomassKT2440_ME
mingrowth	0.043
skipreduction	True
maxreductionsize	30
ignorelistrxns	R-C
popsize	1000
genlimit	100000

Table S3. Properties of the PHA growth-coupled overproducer designs using PET as substrate at 10 mM (2.26 g/L). N.D.: not detected; uptake rate (mmol·gDW^{-1}·h^{-1}); growth rate (h^{-1}); production rate (mmol·gDW^{-1}·h^{-1}); $Y_{p/s,}$ product yield (mmol product/mmol substrate); BCPY, biomass coupled product yield (mmol·gDW^{-1}·h^{-1}). Related to Figure 3.

Design	**Minimal**	**Intermediate**	**Complete**
Uptake rate (mmol·gDW^{-1}·h^{-1})	3.78	3.78	3.78
Knockouts (reactions)	4	8	16
Knockouts (genes)	7	12	27
Growth rate (h^{-1})	0.28	0.21	0.14
Production Rate (min-max)	0 – 0.70	0.90	1.22
Residual Biomass (g/L)	0.75	0.54	0.37
PHA (mM)	N.D.	2.02	3.23
PHA Biomass (g/L)	N.D.	0.32	0.51
Yp/s (mmol PHA/mmol PET)	N.D.	0.20	0.32
BCPY (mmol·gDW^{-1}·h^{-1})	N.D.	0.20	0.17
Biomass PHA (%CDW)	N.D.	37	58

Table S4. *In silico* reactions' nomenclature and essentiality role for coupling PHA to growth. Related to Figure 3.

Reaction	Name	Essentiality for coupling
ORNCD	ornithine cyclodeaminase	High
ICL	isocitrate lyase	High
ICDHyr	isocitrate dehydrogenase	High
MALS	malate synthase	High
FORGLUH2	N-formimino-L-glutamate inimohydrolase	Moderate
MCITL2	methylisocitrate lyase	Moderate
PPCSCT	propanoyl CoA-succinate CoA-transferase	Moderate
SUCOAS	Succinyl-CoA synthetase ADP-forming	Moderate
PDHbr; PDHcr	pyruvate dehydrogenase	Dispensable
UPPN	β-ureidopropionase	Dispensable
ALATA_L	L-alanine transaminase	Dispensable
ALAR	alanine racemase	Dispensable
RBK	ribokinase	Dispensable
OARGDC	oxoarginine decarboxylase	Dispensable
ABUTD	aminobutyraldehyde dehydrogenase	Dispensable

Table S5. Physiological parameters after 24 hours of growth expect otherwise stated under balanced medium conditions. The data correspond to the mean values and standard deviations of at least two biological replicates with the two technical replicates in the methanolysis process. Related to Figures 5-7.

Conditions	Strains	Total biomass (g/L)	PHA (% CDW)	PHA (g/L)	Residual biomass (g/L)
M63 3 mM octa 5 mM 4HBz	KT2440	0.69 ± 0.05	7.09 ± 0.78	0.05 ± 0.01	0.63 ± 0.05
	MM3	0.68 ± 0.05	4.90 ± 1.02	0.03 ± 0.01	0.64 ± 0.04
	MM4	0.63 ± 0.04	4.38 ± 2.04	0.03 ± 0.01	0.60 ± 0.04
	MM6	0.63 ± 0.02	22.56 ± 4.07	0.16 ± 0.03	0.47 ± 0.01
	MM8	0.59 ± 0.01	32.41 ± 2.71	0.19 ± 0.02	0.40 ± 0.02
	MM9	0.57 ± 0.02	31.10 ± 2.07	0.18 ± 0.02	0.39 ± 0.00
	MM11	0.55 ± 0.04	29.05 ± 2.49	0.16 ± 0.00	0.42 ± 0.01
	MM12	0.60 ± 0.03	33.79 ± 2.14	0.19 ± 0.01	0.41 ± 0.02
	MM13	0.57 ± 0.04	32.68 ± 1.15	0.20 ± 0.01	0.40 ± 0.01
	MM14	0.60 ± 0.02	33.53 ± 2.82	0.20 ± 0.02	0.40 ± 0.01
	MM15	0.57 ± 0.04	33.15 ± 3.54	0.20 ± 0.02	0.38 ± 0.01
	MM16	0.59 ± 0.03	33.70 ± 2.47	0.20 ± 0.02	0.39 ± 0.02
	MM19	0.43 ± 0.01	N.D.	N.D.	0.43 ± 0.01
	PP05_01	0.67 ± 0.06	N.D.	N.D.	0.67 ± 0.05
	PP05_01 (pMM55)	0.69 ± 0.03	29.17 ± 3.96	0.20 ± 0.03	0.49 ± 0.05
	MM19 (pMM55)	0.49 ± 0.03	47.39 ± 3.95	0.23 ± 0.02	0.26 ± 0.03
M63 4.4 mM PAC	KT2440	0.32	TR	0.00	0.32
	PP05_01 (pMM55)	0.33	4.13 ± 0.20	0.01	0.31
	MM19 (pMM55)_72 h	0.28	14.67 ± 0.10	0.04	0.24
M63 3.5 mM Ferulic	KT2440	0.37 ± 0.01	TR	TR	0.37 ± 0.01
	PP05_01 (pMM55)	0.38 ± 0.00	7.78 ± 0.94	0.03 ± 0.00	0.35 ± 0.00
	MM19 (pMM55)	0.30 ± 0.00	19.68 ± 0.27	0.06 ± 0.00	0.24 ± 0.00
M63 3.9 mM p-coumaric	KT2440	0.38 ± 0.00	N.D.	N.D.	0.38 ± 0.00
	PP05_01 (pMM55)	0.38 ± 0.01	6.15 ± 0.94	0.02 ± 0.00	0.36 ± 0.01
	MM19 (pMM55)	0.24 ± 0.04	14.23 ± 1.88	0.04 ± 0.01	0.21 ± 0.03
M63 4.4 mM vanillic (48 h)	KT2440	0.27 ± 0.06	N.D.	N.D.	0.27 ± 0.05
	PP05_01 (pMM55)	0.29 ± 0.03	7.68 ± 0.49	0.02 ± 0.00	0.27 ± 0.02
	MM19 (pMM55)	0.26 ± 0.02	15.29 ± 0.33	0.04 ± 0.00	0.22 ± 0.01

M63 5 mM 4HBz	KT2440	0.39 ± 0.02	N.D.	N.D.	0.39 ± 0.01
	MM19	0.34 ± 0.01	N.D.	N.D.	0.34 ± 0.01
	PP05_01	0.39 ± 0.00	N.D.	N.D.	0.39 ± 0.00
	PP05_01 (pMM55)	0.35 ± 0.03	7.12 ± 3.21	0.03 ± 0.01	0.33 ± 0.03
	MM19 (pMM55)	0.31 ± 0.03	19.62 ± 1.46	0.06 ± 0.00	0.26 ± 0.03
Delft 20 mM TPA 20 mM EG_24 h	PP05_18 (pRK190)	1.31 ± 0.05	8.20 ± 0.93	0.11 ± 0.01	1.20 ± 0.03
	MM20 (pRK190)	1.46 ± 0.09	11.00 ± 0.76	0.17 ± 0.02	1.37 ± 0.15
Delft 20 mM TPA 20 mM EG_50 h	PP05_18 (pRK190)	1.09 ± 0.04	8.37 ± 2.18	0.09 ± 0.03	0.99 ± 0.01
	MM20 (pRK190)	1.24 ± 0.02	12.38 ± 4.90	0.15 ± 0.06	1.08 ± 0.06
PET hydrolysate_ 24 h	PP05_18 (pRK190)	1.13 ± 0.15	6.35 ± 1.54	0.07 ± 0.01	1.06 ± 0.14
	MM20 (pRK190)	1.02 ± 0.17	8.63 ± 2.06	0.07 ± 0.01	0.94 ± 0.14
PET hydrolysate_ 50 h	PP05_18 (pRK190)	1.24 ± 0.06	7.14 ± 1.14	0.09 ± 0.01	1.15 ± 0.05
	MM20 (pRK190)	0.98 ± 0.18	11.06 ± 3.11	0.10 ± 0.01	0.88 ± 0.16

Table S6. Defining monomeric PHA composition. The pattern of PHA monomers for the wild type KT2440 and MM16 strains after 24 hours of growth under M63 3 mM 10-undecenoic acid and 5 mM 4-hydroxybenzoate is shown. The data correspond to the mean values and standard deviations of two independent biological replicates with two technical replicates for the methanolysis process. N.D.: not detected. Related to Figure 5.

PHA monomeric composition	Strains	
	KT2440	MM16
% OH-C6	N.D.	N.D.
% OH-C7:1	3.23 ± 2.11	2.46 ± 2.03
% OH-C8	N.D.	N.D.
% OH-C9:1	63.83 ± 2.46	53.47 ± 1.22
% OH-C10	N.D.	N.D.
% OH-C11:1	32.94 ± 1.24	44.07 ± 2.82

Table S7. Selected examples describing mcl-PHA production from lignin-related aromatic substrates using native and engineered pseudomonads strains. In all the cases N limitation was used except in the case of *P. putida* A514 strain (shown by shaded grey color). Related to Discussion section.

Microorganism	Substrate (mM)	Fermentation mode (hours)	CDW (g/L)	PHA (g/L)	PHA (% CDW)	References
P. putida JCM13063	Vanillic acid (59.5)	Batch (72 h)	0.21	Traces	<1	[S11]
P. putida Gpo1	Vanillic acid (59.5)	Batch (72 h)	0.14	Traces	<1	[S11]
P. putida A514	Vanillic acid (14.9)	Batch (50)	0.66	0.01	1.7	[S12]
P. putida A514 Axyl_*alkKphaGC1*	Vanillic acid (14.9)	Batch (50)	0.71	0.25	34.4	[S12]
P. putida A514	Vanillic acid (14.9)	Batch (50)	0.13	0.02	17.3	[S12]
P. putida A514 Axyl_*alkKphaGC1*	Vanillic acid (14.9)	Batch (50)	0.18	0.12	66.3	[S12]
P. putida Gpo1	p-coumaric acid (61)	Batch (72 h)	0.27	Traces	<1	[S11]
P. putida KT2440	p-coumaric acid (12.2)	Batch (48 h)	0.47	0.16	34	[S13]
P. putida KT2440	p-coumaric acid (12.2)	Batch (72 h)	0.38	0.16	41	[S14]
P. putida KT2440 AG2162	p-coumaric acid (12.2)	Fed-Batch (72 h)	0.48	0.24	50	[S14]
P. putida KT2440 AG2162	p-coumaric acid (12.2)	Fed-Batch, HCD (85 h)	1.76	0.95	54.2	[S14]
P. putida Gpo1	Ferulic acid (51.5)	Batch (72 h)	0.15	Traces	<1	[S11]
P. putida KT2440	Ferulic acid (10.3)	Batch (48 h)	0.44	0.17	39	[S13]
P. putida Gpo1	4HBz (72.4)	Batch (72 h)	0.22	Traces	<1	[S11]

REFERENCES

[S1] Bagdasarian, M., Lurz, R., Rückert, B., Franklin, F.C., Bagdasarian, M.M., Frey, J., and Timmis, K.N. (1981). Specific-purpose plasmid cloning vectors. II. Broad host range, high copy number, RSF1010-derived vectors, and a host-vector system for gene cloning in *Pseudomonas*. Gene *16*, 237-247.

[S2] Mato, A., Blanco, F.G., Maestro, B., Sanz, J.M., Pérez-Gil, J., and Prieto, M.A. (2020). Dissecting the Polyhydroxyalkanoate-Binding Domain of the PhaF Phasin: Rational Design of a Minimized Affinity Tag. Appl Environ Microbiol *86*, e00570-20. 10.1128/AEM.00570-20.

[S3] Kessler, B., de Lorenzo, V., and Timmis, K.N. (1992). A general system to integrate lacZ fusions into the chromosomes of gram-negative eubacteria: regulation of the Pm promoter of the TOL plasmid studied with all controlling elements in monocopy. Mol. Gen. Genet. *233*, 293-301.

[S4] Narancic, T., Salvador, M., Hughes, G.M., Beagan, N., Abdulmutalib, U., Kenny, S.T., Wu, H., Saccomanno, M., Um, J., O'Connor, K.E., et al. (2021). Genome analysis of the metabolically versatile *Pseudomonas umsongensis* GO16: the genetic basis for PET monomer upcycling into polyhydroxyalkanoates. Microbial Biotechnology *14*, 2463-2480. 10.1111/1751-7915.13712.

[S5] Schäfer, A., Tauch, A., Jäger, W., Kalinowski, J., Thierbach, G., and Pühler, A. (1994). Small mobilizable multi-purpose cloning vectors derived from the *Escherichia coli* plasmids pK18 and pK19: selection of defined deletions in the chromosome of *Corynebacterium glutamicum*. Gene. 10.1016/0378-1119(94)90324-7.

[S6] Manoli, M.-T., Nogales, J., and Prieto, A. (2022). Synthetic Control of Metabolic States in *Pseudomonas putida* by Tuning Polyhydroxyalkanoate Cycle. mBio *13*, e01794-21. 10.1128/mbio.01794-21.

[S7] Martínez-García, E., and de Lorenzo, V. (2011). Engineering multiple genomic deletions in Gram-negative bacteria: Analysis of the multi-resistant antibiotic profile of *Pseudomonas putida* KT2440. Environmental Microbiology.13, 2702-16 10.1111/j.1462-2920.2011.02538.x.

[S8] Mato, A., Tarazona, N.A., Hidalgo, A., Cruz, A., Jiménez, M., Pérez-Gil, J., and Prieto, M.A. (2019). Interfacial Activity of Phasin PhaF from *Pseudomonas putida* KT2440 at Hydrophobic–Hydrophilic Biointerfaces. Langmuir *35*, 678-686. 10.1021/acs.langmuir.8b03036.

[S9] Wong, S.M., and Mekalanos, J.J. (2000). Genetic footprinting with mariner-based transposition in *Pseudomonas aeruginosa*. Proceedings of the National Academy of Sciences *97*, 10191-10196. 10.1073/pnas.97.18.10191.

[S10] Blázquez, B., Torres-Bacete, J., Leon, D.S., Kniewel, R., Martinez, I., Sordon, S., Wilczak, A., Salgado, S., Huszcza, E., Popłoński, J., et al. (2022). Golden Standard: A complete standard, portable, and interoperative MoClo tool for model and non-model bacterial hosts (Synthetic Biology) 10.1101/2022.09.20.508659.

[S11] Tomizawa, S., Chuah, J.A., Matsumoto, K., Doi, Y., and Numata, K. (2014). Understanding the limitations in the biosynthesis of polyhydroxyalkanoate (PHA) from lignin derivatives. ACS Sustainable Chemistry and Engineering *2*, 1106-1113. 10.1021/sc500066f.

[S12] Wang, X., Lin, L., Dong, J., Ling, J., Wang, W., Wang, H., Zhang, Z., and Yu, X. (2018). Simultaneous Improvements of *Pseudomonas* Cell Growth and Polyhydroxyalkanoate Production from a Lignin Derivative for Lignin-Consolidated Bioprocessing. Appl Environ Microbiol *84*, e01469-18, /aem/84/18/e01469-18.atom. 10.1128/AEM.01469-18.

[S13] Linger, J.G., Vardon, D.R., Guarnieri, M.T., Karp, E.M., Hunsinger, G.B., Franden, M.A., Johnson, C.W., Chupka, G., Strathmann, T.J., Pienkos, P.T., et al. (2014). Lignin valorization through integrated biological funneling and chemical catalysis. Proceedings of the National Academy of Sciences *111*, 12013-12018. 10.1073/pnas.1410657111.

[S14] Salvachúa, D., Rydzak, T., Auwae, R., De Capite, A., Black, B.A., Bouvier, J.T., Cleveland, N.S., Elmore, J.R., Huenemann, J.D., Katahira, R., et al. (2019). Metabolic engineering of *Pseudomonas putida* for increased polyhydroxyalkanoate production from lignin. Microb. Biotechnol., 1751-7915.13481. 10.1111/1751-7915.13481.